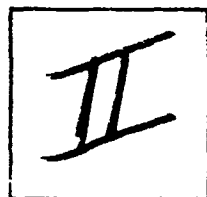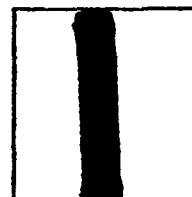AD A122218

DTIC ACCESSION NUMBER

LEVEL

II

INVENTORY

ASD-TR-77-59

DOCUMENT IDENTIFICATION — Final, Jan.'76 – Mar.'77

Edmunds, David B., — Aug.'77

DISTRIBUTION STATEMENT A

Approved for public release;
Distribution Unlimited

DISTRIBUTION STATEMENT

ACCESSION FOR

NTIS	GRA&I	X
DTIC	TAB	☐
UNANNOUNCED		☐
JUSTIFICATION		

BY
DISTRIBUTION /
AVAILABILITY CODES

DIST	AVAIL AND/OR SPECIAL	
A		

DISTRIBUTION STAMP

DTIC
COPY
INSPECTED
2

DTIC
S ELECTE D
APR 26 1983

D

DATE ACCESSIONED

83   04   26   051

DATE RECEIVED IN DTIC

PHOTOGRAPH THIS SHEET AND RETURN TO DTIC-DDA-2

DTIC FORM OCT 79 70A

DOCUMENT PROCESSING SHEET

ASD-TR-77-59

MULTIVARIABLE CONTROL FOR
A VARIABLE AREA TURBINE ENGINE

PERFORMANCE / STABILITY DIVISION
DIRECTORATE OF PROPULSION
PROPULSION DEPUTATE

AUGUST 1977

TECHNICAL REPORT ASD-TR-77-59
Final Report for Period January 1976 — March 1977

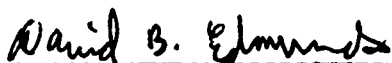Approved for public release; distribution unlimited.

PROPULSION DEPUTATE
AERONAUTICAL SYSTEMS DIVISION
AIR FORCE SYSTEMS COMMAND
WRIGHT-PATTERSON AIR FORCE BASE, OHIO 45433

David B. Edmunds
Aerospace Engineer
Performance/Stability Division
ASD/YZEA

FOR THE COMMANDER

James L. Pettigrew, Lt Col, USAF
Chief, Performance/Stability Division
Directorate of Engineering and Test
Propulsion Deputate

REPORT DOCUMENTATION PAGE		READ INSTRUCTIONS BEFORE COMPLETING FORM
1. REPORT NUMBER ASD-TR-77-59	2. GOVT ACCESSION NO.	3. RECIPIENT'S CATALOG NUMBER
4. TITLE *(and Subtitle)* A MULTIVARIABLE CONTROL FOR A VARIABLE AREA TURBINE ENGINE		5. TYPE OF REPORT & PERIOD COVERED Final Technical Report January 76 - March 77
		6. PERFORMING ORG. REPORT NUMBER
7. AUTHOR(s) David B. Edmunds		8. CONTRACT OR GRANT NUMBER(s)
9. PERFORMING ORGANIZATION NAME AND ADDRESS Aeronautical Systems Division (AFSC) Performance/Stability Division (YZEA) Wright-Patterson AFB, Ohio 45433		10. PROGRAM ELEMENT, PROJECT, TASK AREA & WORK UNIT NUMBERS -328A
11. CONTROLLING OFFICE NAME AND ADDRESS Directorate of Engineering Deputy for Propulsion Wright-Patterson AFB, Ohio 45433		12. REPORT DATE August 1977
		13. NUMBER OF PAGES 90
14. MONITORING AGENCY NAME & ADDRESS*(if different from Controlling Office)*		15. SECURITY CLASS. *(of this report)* UNCLASSIFIED
		15a. DECLASSIFICATION/DOWNGRADING SCHEDULE

16. DISTRIBUTION STATEMENT *(of this Report)*

Approved for public release; distribution unlimited.

17. DISTRIBUTION STATEMENT *(of the abstract entered in Block 20, if different from Report)*

18. SUPPLEMENTARY NOTES

19. KEY WORDS *(Continue on reverse side if necessary and identify by block number)*

Controls, Multivariable control, Variable cycle engine, Turbine engine

20. ABSTRACT *(Continue on reverse side if necessary and identify by block number)*
A multivariable control has been formulated for a turbofan nonaugmented engine with variable area turbines operating at sea level static conditions. The nonlinear dynamic model was represented by two fourth-order linear models. An interactive matrix Ricatti optimization program was developed which automatically calculated a feedback gain matrix and displays on-line the transient response of selected key parameters. The multivariable controller implemented on the nonlinear model required modifications to accommodate both large and small transients gains transitioning and control saturation. Transient results from the controller

DD $\begin{smallmatrix}\text{FORM}\\\text{1 JAN 73}\end{smallmatrix}$ 1473   EDITION OF 1 NOV 65 IS OBSOLETE

are discussed including the effect of component deterioration, sensor and control positioning errors, and installation factors.

TABLE OF CONTENTS

LIST OF TABLES

NOMENCLATURE.

Gas Turbine Parameters

TT25h - gas total temperature downstream of inside diameter fan exit guide vanes.

TT25c - total temperature of gas in duct.

TT3 - total temperature of gas at compressor discharge.

TT4 - total temperature of gas at burner exit.

TT4M - gas temperature at inlet to high pressure turbine.

TT4hi - high turbine gas flow total temperature after energy loss to vanes and blades.

TT4lo - high turbine gas flow total temperature after energy loss to seals and discs.

TT45hi - low turbine gas flow total temperature after energy loss to vanes and blades.

TT45lo - low turbine gas flow total temperature after energy loss to seals and discs.

TT5 - low turbine gas flow exit total temperature.

TT6c - duct exit gas flow total temperature.

TT7 - augmentor exit gas flow total temperature.

PT25c - duct entrance total pressure.

PT3 - compressor discharge total pressure.

PT45 - inter-turbine volume total pressure.

PT7 - afterburner volume total pressure.

PT6c - fan duct volume total pressure.

N1 - fan physical speed.

N2 - compressor physical speed.

AJC - core exhaust nozzle area.

CIVV - fan inlet guide vanes.

RCVV - compressor stator vanes.

WF - main burner fuel flow.

AJD - fan duct exhaust nozzle area.

HTVPOS - high turbine nozzle position.

FTVPOS - fan turbine nozzle position.

FN - net thrust.

WFAN - airflow through fan.

SMAF - fan surge margin.

SMHC - compressor surge margin.

CMVT - Constant Match Varying Temperature.

SECTION I

INTRODUCTION AND BACKGROUND

The majority of present day control systems for gas turbine engines have been derived using classical control techniques. These techniques provided acceptable control systems but required increasingly greater designer skill and time to exploit the full performance capabilities of the more recent variable geometry afterburning turbofan engines (F100-PW-100, GE-F101). Proposed advanced gas turbine engine cycles will have many variable geometry components including fan and compressor vane angles, high and low turbine flow areas, and fan and core exhaust nozzle areas, in addition to fuel flow. This presents the control designer with a complex control system involving multiple inputs and multiple outputs.

Although control modes for such cycles have been derived using classical linear analysis techniques, Beattie (Reference 1), the application of modern control techniques and optimization procedures offers a systematic approach to handle these more complex multivariable problems. For this reason interest in the application of modern control theory to the design and analysis of jet engine controls has increased in recent years. Bowles (Reference 2) and Merrill (Reference 3) studied the application of modern control theory to a single spool turbojet engine. Its application to a two spool turbofan engine has been studied by Michael and Farrar (References 4 and 5) and Weinberg (Reference 6). Finally Beattie (Reference 7) has applied multivariable optimal control techniques to a variable cycle engine (VCE).

These studies have demonstrated that the control laws derived from the optimal control theory can be adapted as a control system on dynamic nonlinear turbine engine models. In all cases the

1

adaptive control system was suboptimal and equal or better than the conventionally designed control in meeting the basic requirements of steady state performance and transient response. The significant conclusion from these studies was that control systems derived using modern control techniques can reduce the design time, trial and error and intuition required relative to classical control techniques. In addition all significant interactions between inputs were accounted for in a systematic manner.

The purpose of this study is the application of modern control techniques and optimization procedures to the design of a controller for a twin spool variable cycle engine. The extent of this study is limited to sea level static conditions for acceleration and deceleration transients of differing magnitudes. Included is a study of the controller's ability to meet steady state performance and transient response requirements when installation and deterioration effects are superimposed on the nonlinear dynamic model.

The design of the controller follows an approach similar to that used by Weinberg (Reference 6). In addition, the original F100-PW-100 dynamic model (Reference 8) was modified to include variable high and low turbine areas, nonmixed duct flow and separate fan duct, and core exhaust nozzles. Steady state control schedules were derived for the sea level static operating condition similar to the standard F100 engine. An interactive computer program was developed to solve the matrix Ricatti equation. The solution is output in the form of the feedback gain matrix and a display of the system response for a particular set of performance index weightings.

2

In summary the objectives of the study are:

1. Modify the original F100-PW-100 transient model to a VCE model and develop the steady state control schedules at the sea level condition.

2. Derive linearized models to represent the nonlinear model at the sea level condition.

3. Derive feedback gains for the multivariable controller based on the linearized models using an interactive Ricatti equation solver computer program.

4. Implement the optimal controller on the nonlinear model in a sub-optimal fashion.

5. Study the controller's performance with installation and deterioration effects.

3

SECTION II

VARIABLE CYCLE ENGINE NONLINEAR MODEL

1. VARIABLE CYCLE ENGINE CONCEPT

Reference 9 presents a detailed study of the benefits of a variable-turbine-geometry turbojet engine versus a fixed-turbine-geometry turbofan engine with comparable capabilities. Reference 1, Section 3 defines the engine cycle for a variable-turbine-geometry turbofan engine with the configuration and engine station designation shown in Figure 1. The increased interest in variable cycle engines (VCE) recently is a result of requirements for both military and super sonic transport (SST) engines to provide extremely high thrust levels while still being capable of operating with low fuel consumption rates at very low power settings for subsonic cruise.

Currently this type of mission profile is satisfied by an after-burning turbofan engine. The afterburner provides the required high thrust levels, while the inherently high propulsive efficiency of the fan provides good performance for subsonic cruise. Total aircraft performance suffers for this engine cycle because of the wide variation of airflows. The engine cycle requires the inlet fan airflow to operate over a wide range between maximum power and cruise conditions. The inlet and nozzle must be sized to accommodate the maximum required airflow rates, resulting in high inlet spillage drag and high aft-end drag at subsonic cruise conditions. The important performance benefit for the VCE configuration over a fixed turbine configuration is the capability to operate at constant fan inlet airflow over not only the augmented power range, but also over a significant portion of the nonaugmented high power range. For example, at the sea level static condition the cycle used in this

4

VARIABLE EXHAUST NOZZLES

VARIABLE TURBINE AREAS

GAS GENERATOR FUEL FLOW

BLEEDS

VARIABLE COMPRESSOR VANES

VARIABLE FAN VANES

CORE AUGMENTOR FUEL FLOW

DUCT AUGMENTOR FUEL FLOW

[13]
[8]
[6]
[5]
[11]
[4]
[3]
[16]
[22]
[13]
[2]

☐ ENGINE STATION DESIGNATIONS
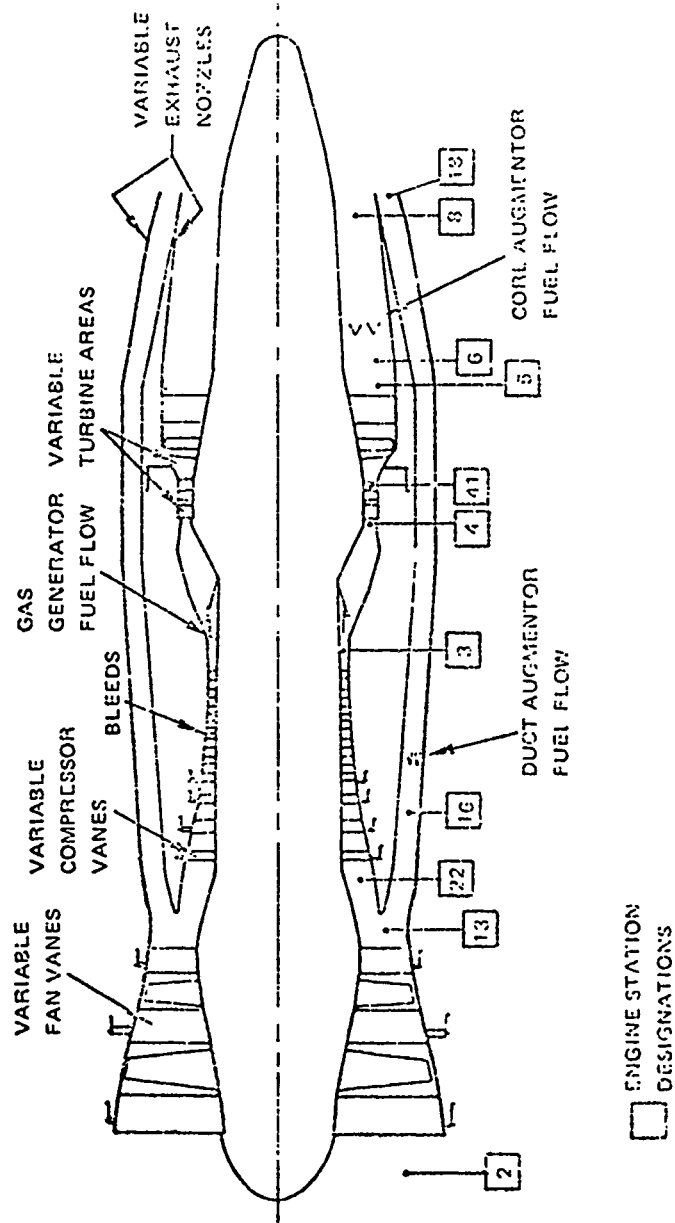
Figure 1. Variable Cycle Engine Schematic

5

study operates at constant fan inlet airflow from 64% to 100% non-augmented thrust.

Constant airflow over this range of thrust levels is accomplished through a mode of operation referred to as constant match varying temperature (CMVT) operation (Reference 1). Both rotor speeds and pressure ratios are held constant as the high pressure turbine stator inlet temperature is varied. As fuel flow is reduced from its maximum value, turbine inlet temperature decreases but the turbines must still maintain a constant value of turbine work. This is accomplished by varying the turbine and core exhaust nozzle areas. The thermodynamic equation governing this process is presented in Appendix A. This mode of operation can continue until the low turbine exit flow parameter reaches a maximum allowable value as determined from consideration of pressure loss and flow separation of the fan turbine exit guide vane. Below this thrust level constant fan and compressor rotor speeds cannot be maintained but with proper scheduling of the fan duct nozzle and fuel flow the desired fan and compressor operating lines and engine bypass ratio can be controlled.

2. NONLINEAR DYNAMIC MODEL

The nonlinear dynamic model used for this study was derived from Pratt and Whitney Aircraft's F100-PW-100 transient engine simulation (Reference 8). This section will describe the original simulation and the next section will describe modifications made to represent the VCE configuration of Figure 1. The engine configuration simulated by the original computer model is depicted in Figure 2. The engine has a three stage fan driven by a two stage low pressure turbine. The fan airflow that bypasses the compressor
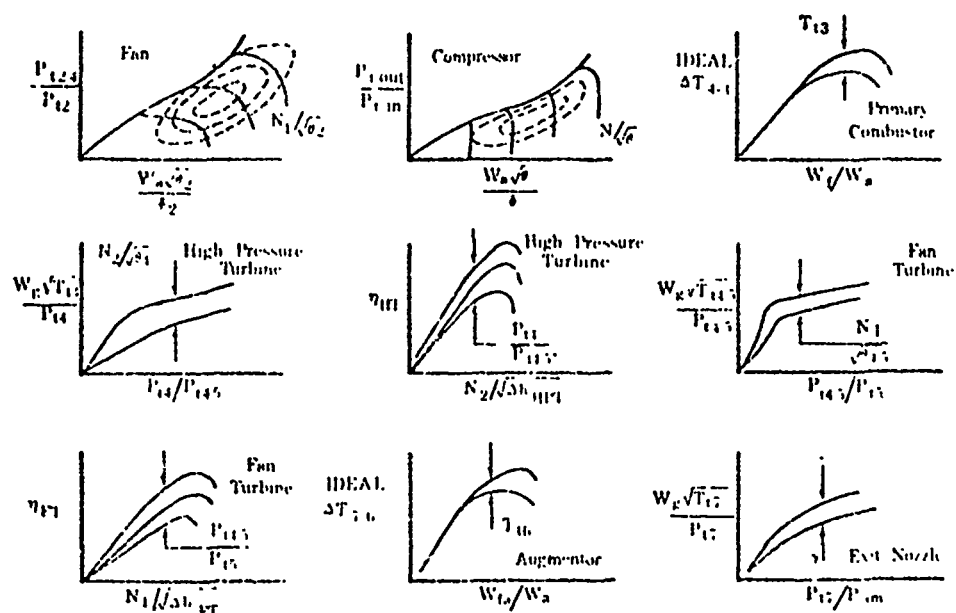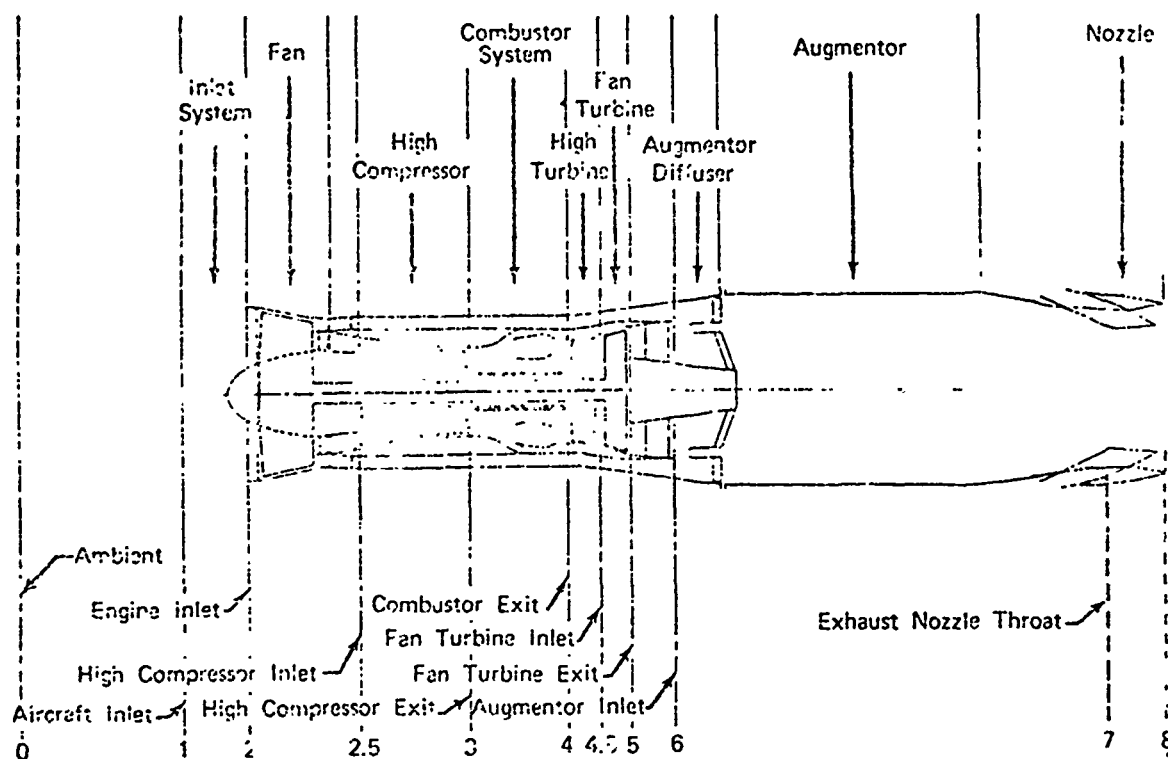
Figure 2. Original F100 Engine Schematic and component
Performance Characteristics (Ref. 8)

is mixed with the low pressure turbine exit flow in the augmentor section and exhausted to ambient conditions through a single variable geometry balance beam nozzle with an actuated divergent flap. This configuration is known as a twin-spool, mixed flow, augmented turbofan engine.

The simulation represents eight basic components, using appropriate aerodynamic and thermodynamic equations relating pressures, temperatures, and mass flows at various stations in the engine and in terms of individual component characteristics as illustrated in Figure 2. The combination of the component characteristics, which are nonlinear, results in a nonlinear model.

The calculation flow path of this simulation is illustrated in Figure 3. A steady state matching point is always calculated first using a modified Newton-Raphson convergence technique (SSMITE). Transient calculations begin at $t=0.0+\Delta t$ and iterated until the input final time is reached. The program takes about 25 seconds Central Processing (CP) time on the CDC 6600 for a one second engine transient.

The engine's dynamics are represented by the seventeen state variables (not including controller dynamics) listed in Table 1. The state variables model the following three dynamic elements:

1. Torque difference integrations which set rotor speeds.

2. First-order temperature lags which represent heat storage.

3. Gas flow difference integrations which set pressures.

These states are controlled by varying the control inputs; main fuel flow, fan and compressor variable geometry, and exit nozzle area.

The engine states are calculated from the recursion formula:

8
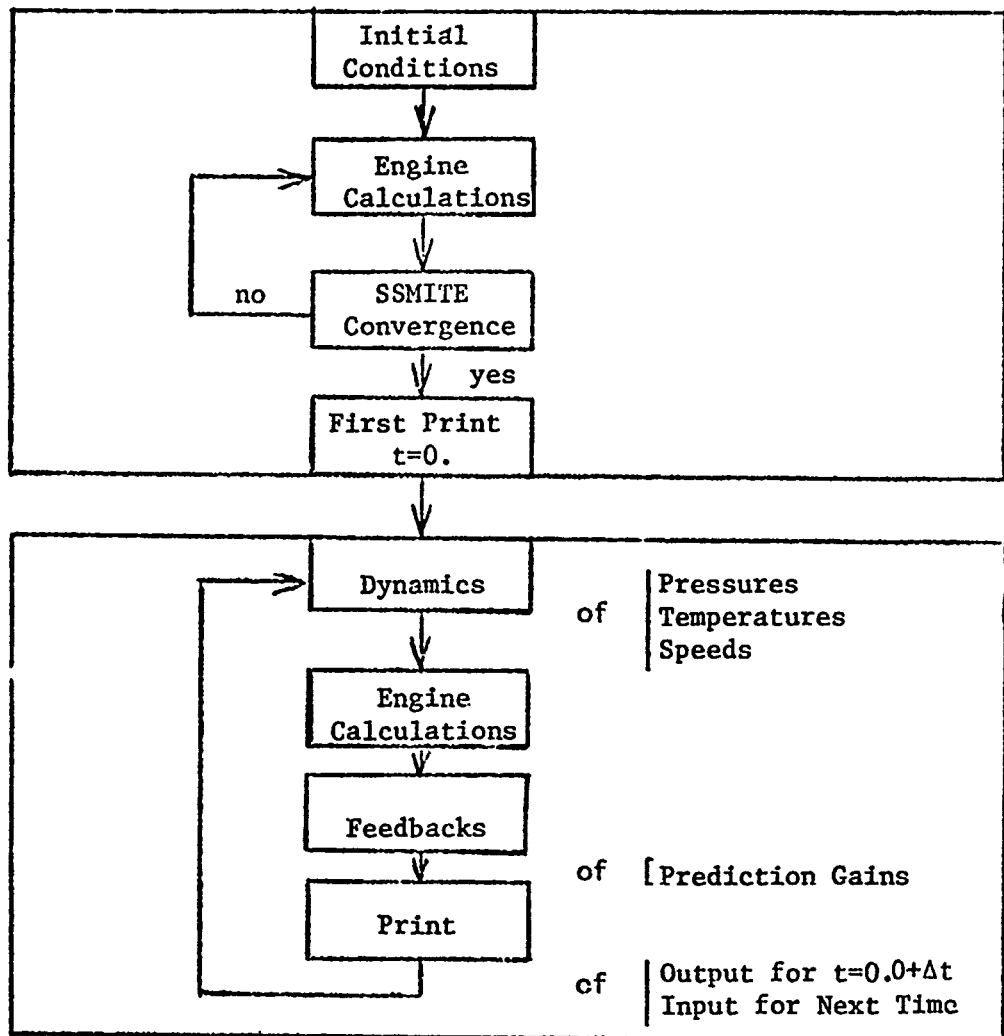
Figure 3. Nonlinear Model Calculation Flow Path

9

TABLE 1

STATE, INPUT, AND OUTPUT VECTORS FOR ORIGINAL F100 MODEL

State Vector

x_1 = gas total temperature downstream of inside diameter fan exit guide vanes (TT25h)

x_2 = total temperature of gas in duct (TT25c)

x_3 = total temperature of gas at compressor discharge (TT3)

x_4 = total temperature of gas at burner exit (TT4)

x_5 = high turbine gas flow total temperature after energy loss to vanes and blades (TT4hi)

x_6 = high turbine gas flow total temperature after energy loss to seals and discs (TT4lo)

x_7 = low turbine gas flow total temperature after energy loss to vanes and blades (TT45hi)

x_8 = low turbine gas flow total temperature after energy loss to seals and discs (TT45lo)

x_9 = low turbine gas flow exit total temperature (TT5)

x_{10} = duct exit gas flow total temperature (TT6c)

x_{11} = augmentor exit gas flow total temperature (TT7)

x_{12} = fan physical speed (N1)

x_{13} = compressor physical speed (N2)

x_{14} = duct entrance total pressure (PT25c)

x_{15} = compressor discharge total pressure (PT3)

x_{16} = inter-turbine volume total pressure (PT45)

x_{17} = afterburner volume total pressure (PT7)

TABLE 1 (concluded)

Input Vector

u_1 = core exhaust nozzle area (AJC)

u_2 = fan inlet guide vanes (CIVV)

u_3 = compressor stator vanes (RCVV)

u_4 = main burner fuel flow (WF)

u_5 = augmentor fuel flow (WFAB)

Output Vector

y_1 = net thrust (FN)

y_2 = gas temperature at inlet to high pressure turbine (TT4M)

y_3 = airflow through fan (WFAN)

y_4 = fan surge margin (SMAF)

y_5 = compressor surge margin (SMHC)

$$x_{i,n+1} = x_{i,n} + \tau_{i,n} \dot{x}_{i,n} [1-e^{-\Delta t/\tau_{i,n}}] \qquad (1)$$

where: $x_{i,n}$ = the ith state after the nth time increment

Δt = time increment

$\tau_{i,n}$ = time constant associated with ith state at the nth

time increment

$\dot{x}_{i,n}$ = the time derivative of the ith state for the nth increment

The time rate of change of the rotor speeds is determined by the difference between the shaft torque generated by the turbine and the shaft torque absorbed by the compressor. These torques are calculated from the turbine and compressor component thermodynamic and aerodynamic relationships. Integration of the turbine-compressor shaft torque difference with respect to time determines the rotor speed for input to the engine calculations of Figure 3.

Temperature dynamics are caused by transient heat storage effects. For example, a temperature change at the inlet to a turbine is not immediately reflected in a change in the energy generated by the turbine, because some of the available energy goes into heating or cooling the turbine disks and blades.

3. VARIABLE CYCLE ENGINE MODEL

The major modifications made to the transient simulation described in the previous section included:

1. Changing the fan duct flow from mixed flow to nonmixed flow. This necessitated the addition of a fan duct exhaust nozzle.

2. High and low pressure turbine flow parameter and efficiency multipliers to simulate the effect of variable turbine geometry.

3. Elimination of afterburner logic.

12

4. Elimination of control scheduling logic and actuator
    dynamics.

5. Addition of steady state control schedules for the sea
    level flight condition used for this study.

The VCE concept has previously been discussed and will not be
repeated in this section. To change the fan duct to a nonmixed
flow configuration required a separate exhaust nozzle for the flow
that bypasses the compressor. The fan duct nozzle calculations were
implemented similar to those for the core nozzle. Both the core
and fan duct exhaust nozzles are variable and are represented by
discharge coefficients and velocity coefficients. The static pressure
balance at Station 6 of Figure 1 required by the original model to
have a balanced steady state condition was eliminated. The elimination
of this allows the fan operating point to be constant in the CMVT
range of operation.

The addition of variable area turbines was accommodated through
multipliers on efficiency and flow parameter as a function of vane
angle. These multipliers are presented in Figure 4. It was assumed
that the turbine design point was at intermediate power (PLA = 83).
There was no unilateral turbine efficiency loss assumed from the
original model. This would most likely not be true for an actual
case but the effect on this study was considered minimal. The
relationships of Figure 4 are simplified best estimates from the
information available. No actual data was available for the cycle
configuration used in this study.

The scope of this study did not include the use of after-
burning which was simulated in the original model. Therefore, the

13
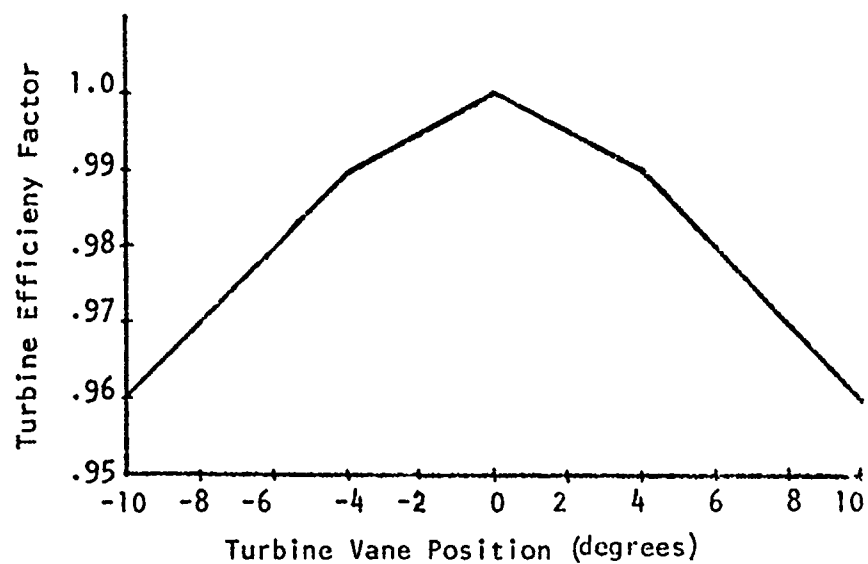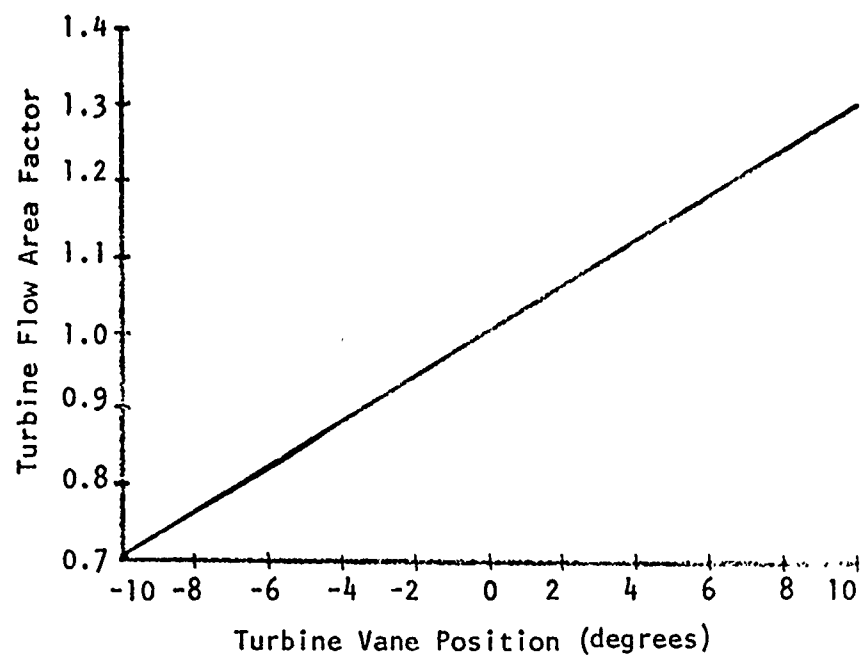
Figure 4. Variable Turbine Efficiency and Flow Area Factors

14

afterburner logic was eliminated to reduce computer memory requirements. The original control scheduling logic and actuator dynamics were also eliminated to reduce the memory size. The VCE simulation derived for this study did not include actuator dynamics. This study represented a preliminary design effort for which the actuator and sensor responses were assumed to be instantaneous. The control designed in this study did not move the actuators instantaneously.

The steady state control schedules derived for this study are shown in Figure 5. These schedules are applicable only at sea level static and were derived based on certain constraints. For the CMVT power range the fan and compressor rotor speeds and pressure ratios were held to the same values of the original model operating at intermediate power (PLA = 83). This resulted in the fan duct exhaust nozzle area (AJD) and fan and compressor vane position (CIVV, RCVV) being constant in the CMVT power range. The relationship between fuel flow (WF) and power level angle (PLA) was arbitrarily established to be approximately the same as in the original model. The two turbines and core nozzle area schedules in the CMVT mode were determined using SSMITE. The three variable areas were allowed to vary until the fan and compressor were operating at the proper match point. These areas were calculated for fuel flows from intermediate power to the CMVT breakpoint. The CMVT breakpoint occurred at PLA = 55, as determined from the considerations mentioned previously.

For power settings below the CMVT breakpoint the two turbines and core nozzle areas were held constant and fan and compressor rotor speeds fell off. The prescribed fan operating line was maintained by allowing the fan duct nozzle to vary and power was reduced by reducing fuel flow. The fan and compressor guide vanes were initially
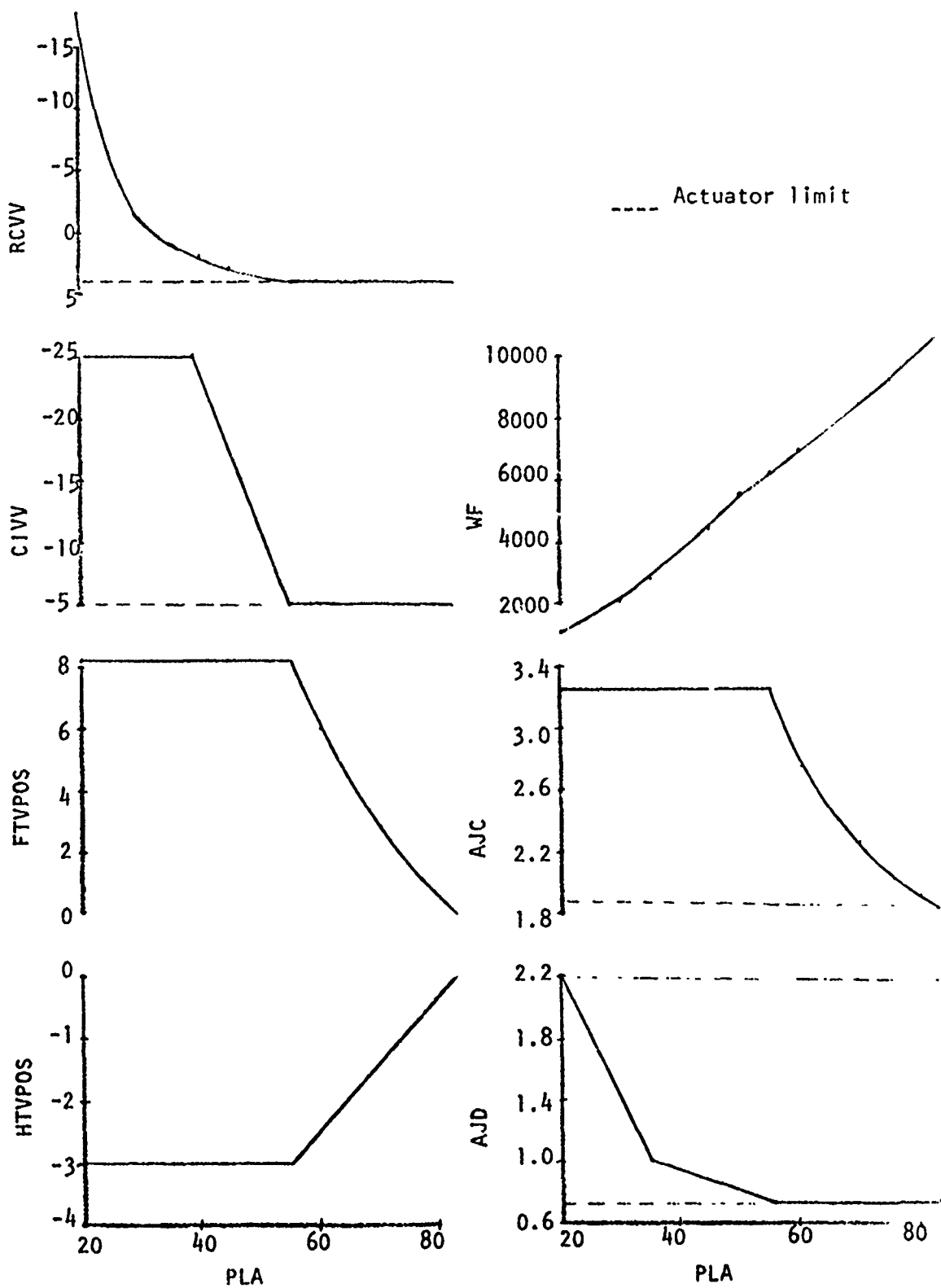
Figure 5. Steady State Control Schedules

16

scheduled as a function of their respective rotor speed using the schedules from the original model. Once the speeds were determined as functions of PLA, the CIVV and RCVV schedules were made a function of PLA instead of speed. This change in the scheduling function was necessitated by the methodology used to derive the multivariable control law (this will be explained in a later section). From a steady state performance standpoint it would be better to schedule the guide vanes as a function of rotor speed.

These steady state schedules make it possible to run the simulation at any power setting (PLA) between 20 and 83 and obtain steady state output. Figure 6 presents plots of some of the output and state variables vs. % intermediate thrust. The rest of this report will discuss a multivariable control that controls the simulation during large or small transients over the entire PLA range.
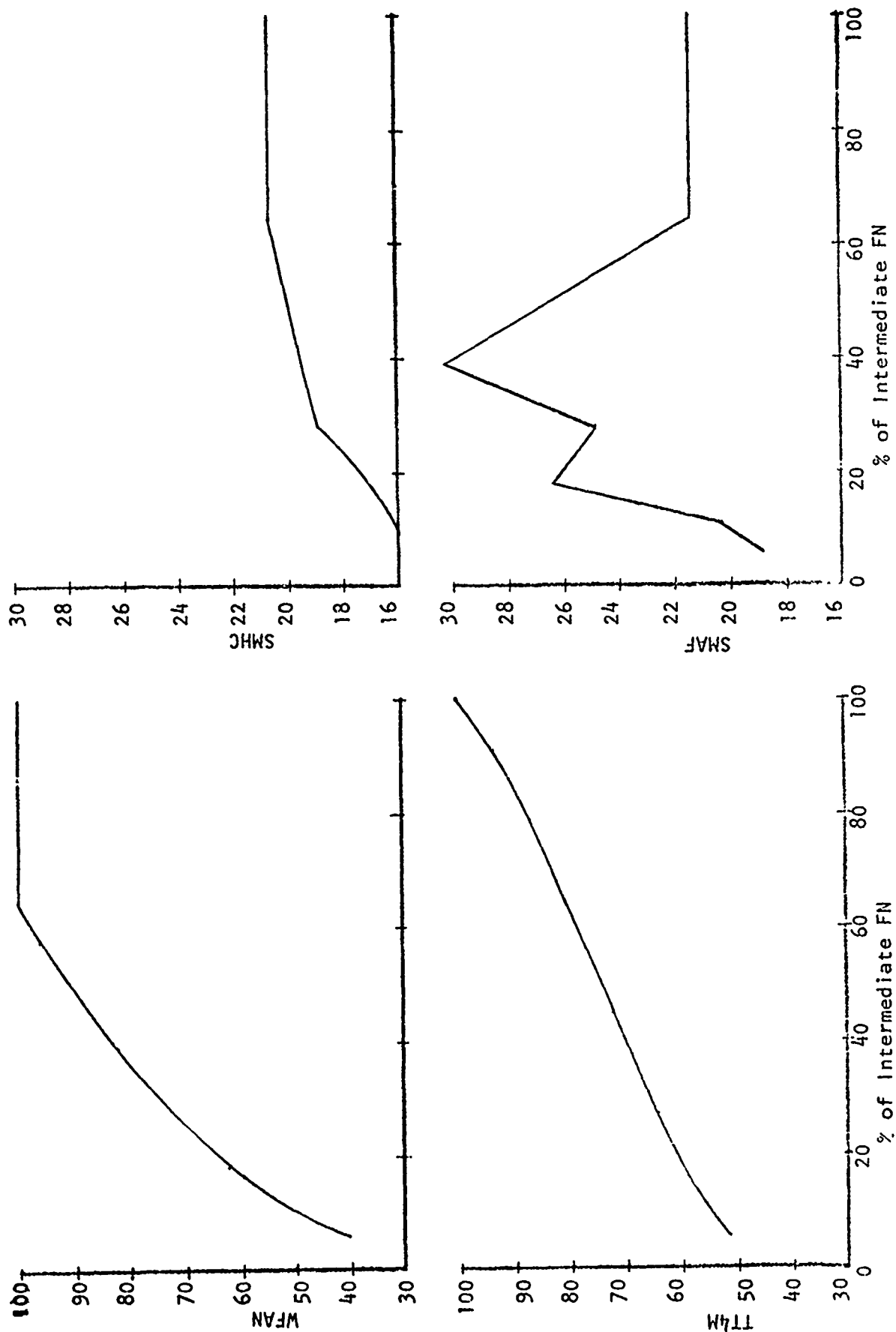
Figure 6. Steady State Output and State Values (% of Intermediate)
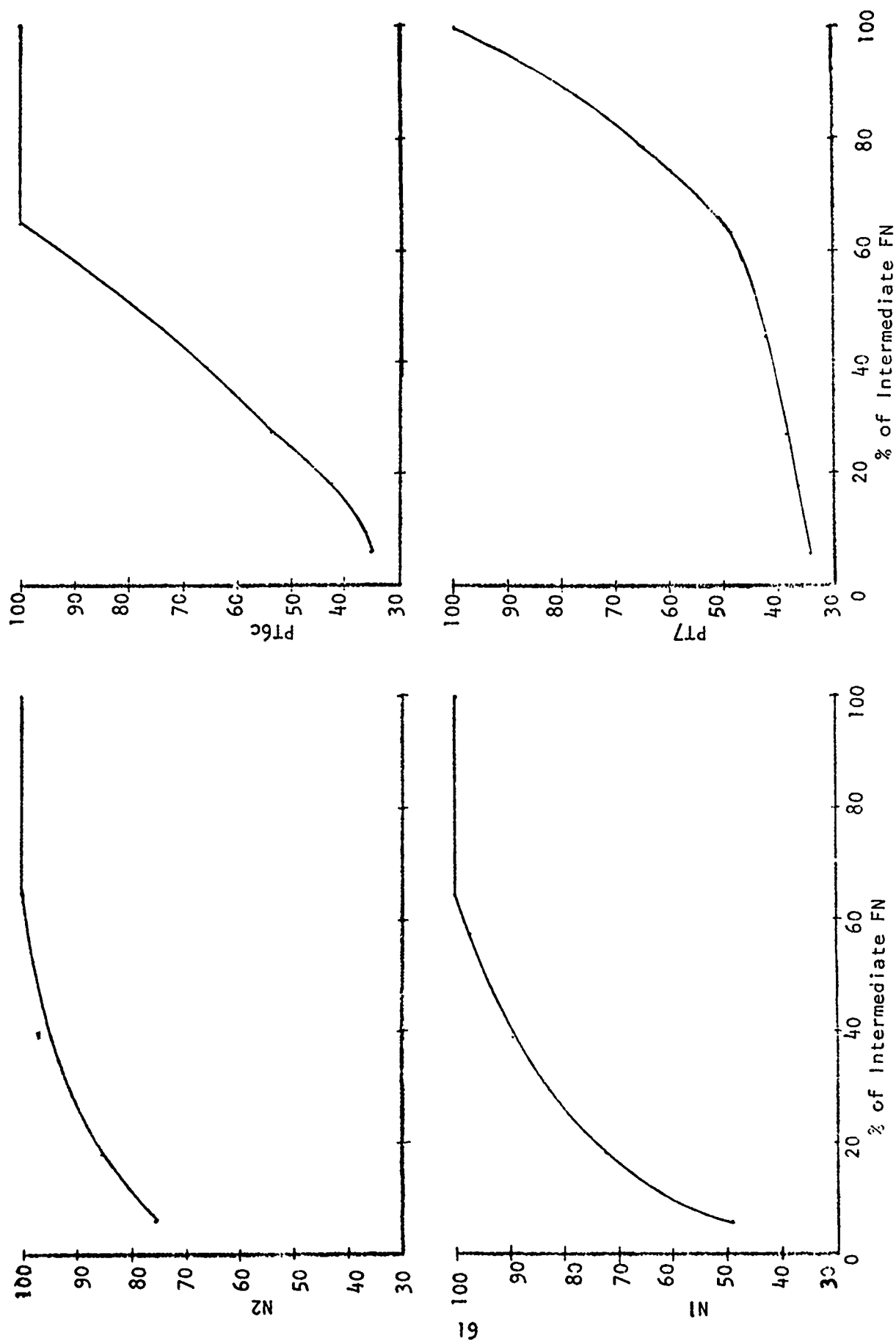
Figure 6. (concluded)

61

SECTION III

CONTROL DESIGN METHODOLOGY

1. LINEARIZATION TECHNIQUE

The variable cycle engine used in this study is represented by the 18 state variables presented in Table 2. This section summarizes a linearization technique developed by Weinberg (Reference 10) which linearizes a high order, nonlinear digital simulation to state variable format by taking partial derivatives of the state variable time derivatives with respect to the states and inputs. The system's eigenvalues are then investigated, as described in the next section, and a reduction is performed so that only the effects of dominant poles remain.

Optimal control theory is based on a mathematical model in state variable form. The state variable form is convenient because the differential equations are ideally suited for digital solution, it provides a unified framework for the study of nonlinear and linear systems and it has strong physical motivation (Reference 11). The linearization converts the eighteen first order nonlinear equations of the VCE simulation indicated by Equation 1 to a linear, time invariant state variable format (Reference 10);

$$\dot{\bar{x}} = \bar{\bar{A}}\bar{x} + \bar{\bar{B}}\bar{u} \tag{2}$$

$$\bar{y} = \bar{\bar{C}}\bar{x} + \bar{\bar{D}}\bar{u} \tag{3}$$

where; $\bar{x}$ = eighteenth order state vector

$\bar{u}$ = seventh order input vector

$\bar{y}$ = fifth order output vector

The overline indicates a vector or matrix, the overdot represents a time derivative. $\bar{\bar{A}}$ is the (18 x 18) matrix of partial derivatives of

20

TABLE 2

STATE, INPUT, AND OUTPUT VECTORS FOR VCE MODEL

State Vector

x_1 = gas total temperature downstream of inside diameter fan exit guide vanes (TT25h)

x_2 = total temperature of gas in duct (TT25c)

x_3 = total temperature of gas at compressor discharge (TT3)

x_4 = total temperature of gas at burner exit (TT4)

x_5 = high turbine gas flow total temperature after energy loss to vanes and blades (TT4hi)

x_6 = high turbine gas flow total temperature after energy loss to to seals and discs (TT4lo)

x_7 = low turbine gas flow total temperature after energy loss to vanes and blades (TT45hi)

x_8 = low turbine gas flow total temperature after energy loss to seals and discs (TT45lo)

x_9 = low turbine gas flow exit total temperature (TT5)

x_{10} = duct exit gas flow total temperature (TT6c)

x_{11} = augmentor exit gas flow total temperature (TT7)

x_{12} = fan physical speed (N1)

x_{13} = compressor physical speed (N2)

x_{14} = duct entrance total pressure (PT25c)

x_{15} = compressor discharge total pressure (PT3)

x_{16} = inter-turbine volume total pressure (PT45)

x_{17} = afterburner volume total pressure (PT7)

x_{18} = fan duct volume total pressure (PT6c)

21

TABLE 2 (concluded)

Input Vector

u_1 = core exhaust nozzle area (AJC)

u_2 = fan inlet guide vanes (CIVV)

u_3 = compressor stator vanes (RCVV)

u_4 = main burner fuel flow (WF)

u_5 = fan duct exhaust nozzle area (AJD)

u_6 = high turbine nozzle position (HTVPOS)

u_7 = fan turbine nozzle position (FTVPOS)

Output Vector

y_1 = net thrust (FN)

y_2 = gas temperature at inlet to high pressure turbine (TT4M)

y_3 = airflow through fan (WFAN)

y_4 = fan surge margin (SMAF)

y_5 = compressor surge margin (SMHC)

the state time derivatives with respect to the states;

$$
\bar{A} = \begin{vmatrix}
\dfrac{\partial \dot{x}_1}{\partial x_1} & \dfrac{\partial \dot{x}_1}{\partial x_2} & \cdot & \cdot & \cdot & \cdot & \cdot & \cdot & \cdot & \dfrac{\partial \dot{x}_1}{\partial x_{18}} \\
\\
\dfrac{\partial \dot{x}_2}{\partial x_1} & \dfrac{\partial \dot{x}_2}{\partial x_2} & \cdot & \cdot & \cdot & \cdot & \cdot & \cdot & \cdot & \dfrac{\partial \dot{x}_2}{\partial x_{18}} \\
& & & & & & & & & \cdot \\
& & & & & & & & & \cdot \\
\cdot & & & & & & & & & \cdot \\
\\
\dfrac{\partial \dot{x}_{18}}{\partial x_1} & \cdot & \cdot & \cdot & \cdot & \cdot & \cdot & \cdot & \cdot & \dfrac{\partial \dot{x}_{18}}{\partial x_{18}}
\end{vmatrix}
\tag{4}
$$

where: $\quad \dot{x}_{i,n+1} = \dfrac{x_{i,n+1} - x_{i,n}}{\Delta t}$ (4a)

$$
\dfrac{\partial \dot{x}_i}{\partial x_i} = \dfrac{\dot{x}_{i,n+1} - \dot{x}_{i,n}}{x_{i,n+1} - x_{i,n}}
\tag{4b}
$$

Δt = time increment

$x_{i,n}$ = the value of the ith state before the integration

$x_{i,n+1}$ = the value of the ith state after the integration

$\bar{B}$ is the (18x7) matrix of partial derivatives of the state time derivatives with respect to the inputs;

$$
\bar{B} = \begin{vmatrix}
\dfrac{\partial \dot{x}_1}{\partial u_1} & \cdot & \cdot & \cdot & \cdot & \cdot & \dfrac{\partial \dot{x}_1}{\partial u_7} \\
& \cdot & & & & & \cdot \\
& \cdot & & & & & \cdot \\
& \cdot & & & & & \cdot \\
\dfrac{\partial \dot{x}_{18}}{\partial u_1} & \cdot & \cdot & & \cdot & & \dfrac{\partial \dot{x}_{18}}{\partial u_7}
\end{vmatrix}
\tag{5}
$$

23

$\bar{C}$ is the (5x18) matrix of partial derivatives of the outputs with respect to the states;

$$\bar{C} = \begin{vmatrix} \dfrac{\partial y_1}{\partial x_1} & \cdot & \cdot & \cdot & \cdot & \cdot & \dfrac{\partial y_1}{\partial x_{18}} \\ \cdot & & & & & & \cdot \\ \cdot & & & & & & \cdot \\ \cdot & & & & & & \cdot \\ \dfrac{\partial y_5}{\partial x_1} & \cdot & \cdot & \cdot & \cdot & \cdot & \dfrac{\partial y_5}{\partial x_{18}} \end{vmatrix} \qquad (6)$$

$\bar{D}$ is the (5x7) matrix of partial derivatives of the outputs with respect to the inputs;

$$\bar{D} = \begin{vmatrix} \dfrac{\partial y_1}{\partial u_1} & \cdot & \cdot & \cdot & \cdot & \cdot & \dfrac{\partial y_1}{\partial u_7} \\ \cdot & & & & & & \cdot \\ \cdot & & & & & & \cdot \\ \cdot & & & & & & \cdot \\ \dfrac{\partial y_5}{\partial u_1} & \cdot & \cdot & \cdot & \cdot & \cdot & \dfrac{\partial y_5}{\partial u_7} \end{vmatrix} \qquad (7)$$

The basic strategy used to calculate the state matrices of Equations 4 thru 7 was to converge on a steady-state condition and then perturb, one at a time, each of the state and input variables. The nonlinear dynamic simulation was modified to incorporate the following algorithm for calculating the linearized state matrices;

1. A steady state point at PLA = 83 is run to obtain the normalizing values.

2. A steady state point at the desired power setting is run to

24

obtain $x_{i,n}$ (the choice of power settings will be discussed later).

3. Each of the state and input variables (25 in all) are perturbed one at a time from their steady-state values and the transient simulation run for fifty time steps to obtain $x_{i,n+1}$ of the $\bar{A}$ and $\bar{B}$ matrices in Equations 4 and 5.

4. The $\bar{C}$ and $\bar{D}$ matrices of Equations 6 and 7 are calculated in a similar manner as for $\bar{A}$ and $\bar{B}$; however, no integrations were required to perform the derivative calculations of Equations 6 and 7.

The derivatives were calculated from 50 time steps of 0.00001 seconds each. The state and input variables were usually incremented 0.2% of their base values. Once calculated these matrices were punched out on cards in a format suitable for input to the matrix reduction program discussed in the next section. For more specific details of the above procedure see Reference 10.

2. MATRIX REDUCTION

To facilitate the analysis and design of dynamic control systems, it is often desirable to reduce the system's order. In linear systems, this reduction is possible when the system's transfer function contains dominant poles which determine the transient response essentially independently of the remaining poles (Reference 12). In the complex plane, the less dominant poles appear to the left of the dominant poles and represent transient terms which die quickly when compared to the transient terms associated with the dominant poles. This section summarizes a technique developed by Weinberg (Reference 12). which reduces a high order system to a lower order system, whose

25

poles correspond to the dominant poles of the higher order transfer function. This reduction technique does not require previous knowledge of system characteristics and identifies important dynamic states in a straight-forward manner.

The values of the $\bar{A}$, $\bar{B}$, $\bar{C}$ and $\bar{D}$ for the 18th order linearized modes are given in Table 3. An algorithm (References 10 and 12) to reduce the order of the model is summarized below.

Recalling the state variable form of Equations 2 and 3 it is assumed that the matrix $\bar{A}$ has r nondominant poles which can be eliminated, implying that r states of $\bar{x}$ have zero derivatives.

$$\dot{\bar{x}} = \bar{A}\bar{x} + \bar{B}\bar{u} \tag{8}$$

$$\bar{y} = \bar{C}\bar{x} + \bar{D}\bar{u} \tag{9}$$

Equations 8 and 9 can be rewritten with partitioned matrices;

$$\left|\begin{array}{c} \dot{\bar{x}}_{p1} \\ \hline \dot{\bar{x}}_{p2} \end{array}\right| = \left|\begin{array}{c|c} \bar{A}_{p11} & \bar{A}_{p12} \\ \hline A_{p21} & A_{p22} \end{array}\right| \left|\begin{array}{c} \bar{x}_{p1} \\ \hline x_{p2} \end{array}\right| + \left|\begin{array}{c} \bar{B}_{p1} \\ \hline B_{p2} \end{array}\right| \bar{u} \tag{10}$$

$$\bar{y} = \left|\begin{array}{cc} \bar{C}_{p1} & \bar{C}_{p2} \end{array}\right| \left|\begin{array}{c} \bar{x}_{p1} \\ \hline \bar{x}_{p2} \end{array}\right| + \bar{D}\,\bar{u} \tag{11}$$

where: $\bar{x}_{p1}$ = (n-r)x1 vector whose derivatives $\dot{\bar{x}}_{p1}$ are dynamically important

$\dot{\bar{x}}_{p2}$ = (rx1) vector whose derivatives $\dot{\bar{x}}_{p2}$ are dynamically insignificant

$\bar{A}_{p11}$ = (n-r)x(n-r) matrix

$\bar{A}_{p12}$ = (n-r)xr matrix

$\bar{A}_{p21}$ = rx(n-r) matrix

$\bar{A}_{p22}$ = (rxr) matrix

TABLE 3

18th Order Linearized Matrices for PLA=60

A MATRIX

VARIABLE 1
```
-19.54450     .10130    -.0003.    -.00266    .003+0    0.00000    .00320    .10040
-0.00000     0.90000   -0.60366    6.33060   -.06350    2.94320    .00080    .10660
-.00439      .06760
```

VARIABLE 2
```
-.19303    -19.49770    0.60030     .00030     .00010    0.00000   -.00050   -.00010
 0.00000     .95013     0.00000     .32570     .22520    9.91350   -.00036   -.00120
 .00070      .05030
```

VARIABLE 3
```
 14.62100    -.00120    -19.65050    .05430     .06490    .00060    -0.00000   -0.00000
 0.00000    -0.30000     0.06000    -.01100    7.01410   -2.77470    4.16030   -.00290
 0.00000    -.04520
```

VARIABLE 4
```
 18.90150    -.06440     19.01443   -47.61010   -.01340   -.50150    -.00010   -0.00000
 0.00000    -.60010     0.09007    -.09600    -20.32670  -10.23590    .03420     .00760
 .50010     -.10030
```

VARIABLE 5
```
 .32480     -.00010     3.47970     45.44010   -49.33030  -0.00000   -0.00000   -0.00000
 0.00000    -0.50000     0.50000    -.00170    -.22030    -.17650     .00400     .00010
 0.00000    -.06220
```

VARIABLE 6
```
 .00440     -0.00000     .04700     .61400    -0.00000   -.06560    -0.00000    0.00000
 0.00000    -0.30000     0.00000   -0.00000   -.00300    -.00240     .00010    0.10000
 0.00000    -0.10000
```

VARIABLE 7
```
 .24600     -0.00000     6.75270     50.17010   -15.35930  -1.74950   -43.33010    0.00000
 0.00000     0.05000    -0.00000     .03590    -2.23030   -.12590    -0.95610    0.05970
-0.00000    -.30700
```

VARIABLE 8
```
 .00390     -0.00000     .27370     2.43020    -.62930    -.07080    9.00000    -1.49900
 0.00000     0.50000     0.00000     .00350    -.09260    -.00510    -.28130     .54270
-0.00000    -0.00000
```

VARIABLE 9
```
 .24100     -0.00000     3.49000     29.75530   -7.00710   -.35000    -4.23670   -.07530
-19.90030   -0.30000     .00350    -.63590    -1.25010   -.12910    -3.87400    .01740
 5.49530    -.00120
```

VARIABLE 10
```
-.42000     13.49300     .23330     .03370     .00030    0.00000    -.00020   -0.00000
 0.00000    -19.30030    0.00000    -.256.0     .46470     .27290    -.00030   -.10050
 .00020      .00-20
```

VARIABLE 11
```
 .01930     -2.00000     .15810     .37480    -.09470    -.01050    -.05170    -.10560
 49.01370   -0.30000    -45.35020   -.03590    -.03350    -.01080    -.04950    -.00200
 .90500     -.00020
```

VARIABLE 12
```
-.07740     -.00036     -.21010    -1.33170     .30070     .03390    2.24110     .25190
-0.00000    -0.00000    -.00130    -2.53400     .12640    -1.25170     .65910    4.05590
-2.33570    -.02030
```

VARIABLE 13
```
 1.63340    -.00000     -.32900    -1.27170    2.65740     .33000    -0.00000   -0.00000
 0.00000    -0.00000     0.00000    -.02440    -5.29910   -.99490    2.63700    -1.05130
 0.00000    -.01630
```

VARIABLE 14
```
 6.78450    1.79500     -.00010     .00040    -.00430    -.00050     .00410     .00050
 0.00000     .03390    -0.09000    8.71470    -7.71930   -73.03010    .00860     .01060
-.00010     02.04440
```

VARIABLE 15
```
-144.59400    .03710    16.95290    53.33570     .10950     .01230     .00050     .10010
 0.00000     .00010    -0.60000     .77640    165.06930   32.91030  -127.45550   -.05150
-.00060     1.74740
```

VARIABLE 16
```
-42.03100    .06940    -23.74920    143.22670   -31.01210   -9.11740    .01930     .10220
-0.00010     .00020    -0.60000     34.20140    36.92340   23.85830   356.08930  -546.50700
-.02510     .55700
```

VARIABLE 17
```
-.06770     0.00000     -.32850    -2.37870     .56260     .05330    -.00020    -0.00000
 .03070     0.00000     2.51070    -.23560     .14910     .03750     .76150     3.79460
-7.10190     .00000
```

VARIABLE 18
```
 12.10120    .31230     -.02300     .02850    -.00790    -.00090     .00750     .00080
-0.00000    3.33170    -0.00000    12.03220   -13.77400   -7.03930    .01510     .01940
-.00940    -5.71000
```

TABLE 3 (continued)

B MATRIX
VARIABLE 1
      C.00000   -.54.70   .014°C   -0.00000   -0.00000   -.00010   -.00040
VARIABLE 2
     -0.00000   -.334.30   -.C5050   0.00000   -.00010   -0.00000   .00010
VARIABLE 3
     -0.00000   .00370   -.23410   .00320   0.00500   .03780   -.00010
VARIABLE 4
     -0.00000   .01070   4.54290   23.83990   .00020   .00430   .00020
VARIABLE 5
      0.00000   .00030   .07840   .43050   0.00000   .00013   0.00000
VARIABLE 6
      0.00000   0.00000   .00110   .00570   0.00000   0.00000   0.00000
VARIABLE 7
      0.00000   .00020   .05020   1.11030   -0.00000   -.00550   .29030
VARIABLE 8
      0.00000   0.00000   .00220   .04520   -0.00000   -.00340   .01170
VARIABLE 9
     -.00320   .00020   .05730   .65310   0.00000   .05960   -.17040
VARIABLE 10
     -0.00000   .03510   -.11730   .00050   -0.00000   -.00010   0.00000
VARIABLE 11
     -0.00000   0.00000   .00470   .04200   0.00000   .00170   -.00030
VARIABLE 12
      .00170   .32200   -.01040   -.01600   0.00000   -.10000   -.27420
VARIABLE 13
     -0.00000   .00100   .05550   -.00730   0.00000   -.74510   -.04960
VARIABLE 14
      0.00000   -.90000   1.72170   -0.00000   -.10570   .00140   -.00050
VARIABLE 15
      0.00000   -.13400   -20.00070   3.15090   -.00140   35.70160   -.00140
VARIABLE 16
      0.00000   -.03560   -10.03610   5.15770   -.00040   -110.90200   113.34470
VARIABLE 17
     -2.41890   -.00010   -.01600   -.02750   -0.00000   -.14430   -.76730
VARIABLE 18
      0.00000   -1.757-0   3.07160   .00020   -6.60930   .00250   -.06090

C MATRIX
VARIABLE 1
     -.00110   0.00000   0.00000   0.00000   0.00000   .00000   0.00000   0.00000
      0.00000   -.00510   -.00110   0.00000   .00110   .00000   -0.00000   0.00000
      1.54550   .09000
VARIABLE 2
      .00220   0.00000   .00630   .93210   0.00000   0.00000   0.00000   0.00000
      0.00000   0.00000   0.00000   -0.00000   .00010   -.00130   0.00000   0.00000
      0.00000   0.00000
VARIABLE 3
     -.00010   0.00000   0.00000   0.00010   0.00000   0.00000   0.00000   0.00000
      0.00000   0.00000   0.00010   .70950   .00020   -.00760   -0.00000   0.00000
      0.00000   0.00000
VARIABLE 4
     -.01130   0.00000   0.00000   0.00000   0.00000   0.00000   0.00000   0.00000
      0.00000   0.00000   0.00000   1.71030   .01230   -.04520   -0.00000   0.00000
      0.00000   0.00000
VARIABLE 5
     -.99270   0.00000   0.00000   0.00000   0.00000   0.00000   0.00000   0.00000
      0.00000   0.00000   0.00000   .00030   1.76290   .04920   -.79730   0.00000
      0.00000   0.00000

D MATRIX
VARIABLE 1
      .29370   -0.00000   -.00020   -.00130   .25290   0.00000   0.00000
VARIABLE 2
      0.00000   0.00000   .00060   .00300   0.00000   0.00000   0.00000
VARIABLE 3
      0.00000   -.10310   -0.00000   0.00000   0.00000   0.00000   0.00000
VARIABLE 4
      0.00000   -.12530   -.00230   0.00010   0.00000   0.00000   0.00000
VARIABLE 5
      0.00000   -.00010   -.20000   0.00010   0.00000   0.00000   0.00000

$$\bar{B}_{p1} = (n-r)xm \text{ matrix}$$

$$\bar{B}_{p2} = (r-m) \text{ matrix}$$

$$\bar{C}_{p1} = px(n-r) \text{ matrix}$$

$$\bar{C}_{p2} = (pxr) \text{ matrix}$$

$$\bar{D} = (pxm) \text{ matrix}$$

n = number of states (18)

m = number of control inputs (7)

p = number of outputs (5)

r = number of non-dominant poles

Reference 12, Appendix A presents an algorithm for converting a set of state equations into the form of Equations 10 and 11. Setting $\dot{x}_{p2} = 0$, the reduced state equations become;

$$\dot{x}_{p1} = \bar{A}_r \bar{x}_{p1} + \bar{B}_r \bar{u} \tag{12}$$

$$\bar{y} = \bar{C}_r \bar{x}_{p1} + \bar{D}_r \bar{u} \tag{13}$$

where:
$$\bar{A}_r = \bar{A}_{p11} - \bar{A}_{p12} \bar{A}_{p22}^{-1} \bar{A}_{p21}$$
$$\bar{B}_r = \bar{B}_{p1} - \bar{A}_{p12} \bar{A}_{p22}^{-1} \bar{B}_{p2}$$
$$\bar{C}_r = \bar{C}_{p1} - \bar{C}_{p2} \bar{A}_{p22}^{-1} \bar{A}_{p21}$$
$$\bar{D}_r = \bar{D} - \bar{C}_{p2} \bar{A}_{p22}^{-1} \bar{B}_{p2}$$

Equations 12 and 13 completely define the reduced system model but the state derivatives of $\dot{x}_{p2}$ must be determined before the reduction can be performed. The eigenvalues for the VCE system are given in Table 4. Eigenvalues with real parts less than -15 are considered to be nondominant poles. It is observed that the system derived in this study has six dynamically important poles.

Summarizing, to determine the unimportant state derivatives of $\dot{x}_{p2}$ the following procedure was used;

TABLE 4

EIGENVALUES OF A MATRIX FOR PLA = 60

18th order	6th order	4th order
-547.08	-12.27	-12.34
-130.03	-0.66	$-3.66\pm1.57j$
-64.68	$-3.70\pm1.55j$	-3.65
-57.12	-3.64	
-50.92	-2.00	
-49.38		
-36.24		
$-24.47\pm6.45j$		
-22.54		
$-18.58\pm3.53j$		
-9.56		
$-3.65\pm1.81j$		
-3.04		
-0.66		
-1.99		

1. Assume that a pole (or poles) is nondominant.

2. Rearrange $\bar{x}$ into the submatrices $\bar{x}_{p1}$ and $\bar{x}_{p2}$.

3. Rearrange $\bar{A}$, $\bar{B}$, and $\bar{C}$ to correspond to the new order of $\bar{x}$.

4. Calculate the reduced matrix $\bar{A}_r$ and determine its eigenvalues.

5. If $\bar{x}_{p2}$ consists of only derivatives corresponding to non-dominate poles, the dominant poles of $\bar{A}_r$ will approximate the dominant poles of $\bar{A}$.

A program from Reference 12 was used to automatically perform steps 2 thru 4. The calculated eigenvalues for a sixth order system and a fourth order system are presented in Table 4. The states used in the submatrix $\bar{x}_{p1}$ for the sixth and fourth order systems are presented in Table 5. These are the states that, when individually substituted as $\bar{x}_{p2}$ into the matrix reduction program, caused the dominant poles to shift. The resulting $\bar{A}$, $\bar{B}$, $\bar{C}$, and $\bar{D}$ matrices for the sixth and fourth order systems are presented in Table 6.

The reduction from six to four states was possible because two of the states had no effect on the output variables as evidenced by the two columns of near zero values in the $\bar{C}$ matrix, 6th order, of Table 6. This is further demonstrated in Figure 7 where the output variables of the 18th, 6th, and 4th order linear models and the output of the nonlinear model are plotted for a step input in fuel flow. The actual engine is, in this case, modeled by 18 states that denote energy storage. The four states identified by the reduction program are the states which store energy sufficient enough to affect the engine's transient performance. The fourth order model at two different power settings was used for this study to derive a multivariable control as described in later sections.

31

TABLE 5

STATE VECTORS FOR 6TH AND 4TH ORDER MODELS

6th order

x_1 TT411o $-(x_6)$- high turbine gas flow total temperature after energy

loss to vanes and blades

x_2 TT451o $-(x_8)$- low turbine gas flow total temperature after energy

loss to seals and discs

x_3 N1 $-(x_{12})$- fan physical speed

x_4 N2 $-(x_{13})$- compressor physical speed

x_5 PT7 $-(x_{17})$- afterburner volume total pressure

x_6 PT6c $-(x_{18})$- fan duct volume total pressure

4th order

x_1 N1 $-(x_{12})$- fan physical speed

x_2 N2 $-(x_{13})$- compressor physical speed

x_3 PT7 $-(x_{17})$- afterburner volume total pressure

x_4 PT6c $-(x_{18})$- fan duct volume total pressure

( )- state variable number from Table 2

TABLE 6

6TH AND 4TH ORDER LINEARIZED MATRICES FOR PLA=60

6th order

A MATRIX
VARIABLE 1

C MATRIX
VARIABLE 1

B MATRIX
VARIABLE 1
VARIABLE 2
VARIABLE 3
VARIABLE 4
VARIABLE 5
VARIABLE 6

D MATRIX
VARIABLE 1
VARIABLE 2
VARIABLE 3
VARIABLE 4
VARIABLE 5
VARIABLE 6

4th order

A MATRIX
VARIABLE 1

C MATRIX
VARIABLE 1

B MATRIX
VARIABLE 1
VARIABLE 2
VARIABLE 3
VARIABLE 4

D MATRIX
VARIABLE 1
VARIABLE 2
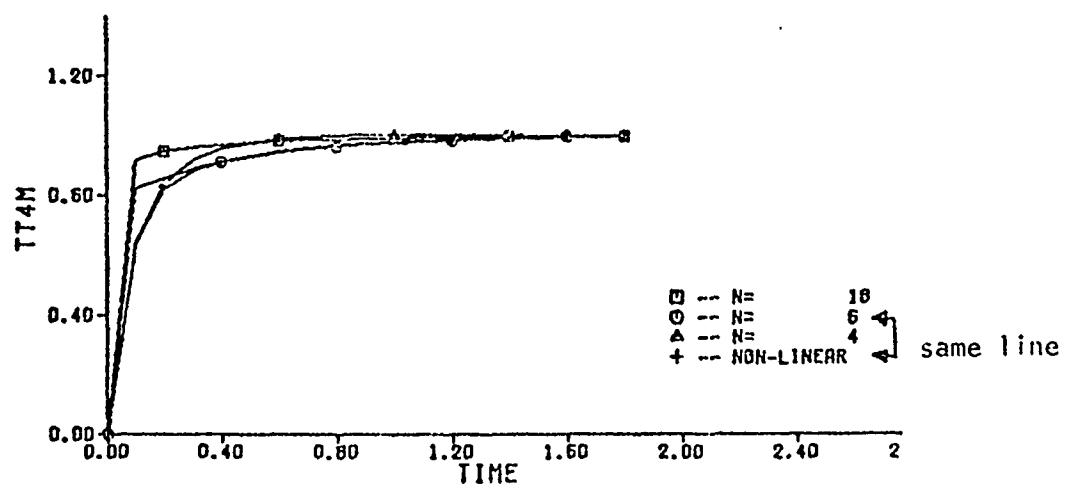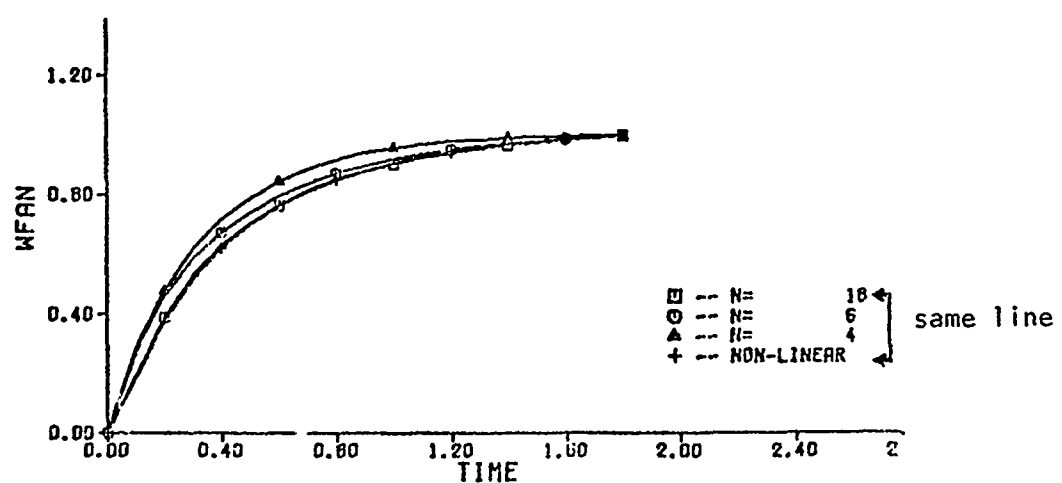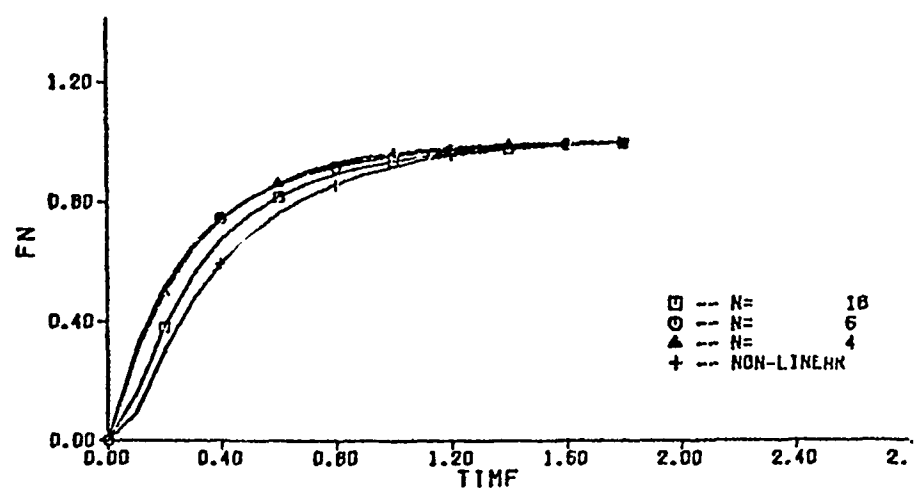VARIABLE 3
VARIABLE 4
VARIABLE 5

33

Figure 7. Comparison of Linear Models with Nonlinear Model for
Small Step Change in Fuel Flow (WF)

34

3. CONTROL OPTIMIZATION TECHNIQUE FOR LINEARIZED MODELS

As stated in the introduction, the design of a multi-input, multi-output control system using classical techniques requires a significant amount of trial-and-error, experience and intuition. The purpose of this study was to further demonstrate the application of optimization techniques as a design tool for multivariable control systems. This section will discuss some of these optimization techniques and their application to the control design for the VCE.

The objective of optimal control theory is to determine the control signals that will cause a process to satisfy the physical constraints and at the same time minimize some performance criterion (Reference 11). For the variable area turbine engine, some of the physical constraints include fan and compressor surge margins, maximum turbine inlet temperature level and rate of change, maximum pressure levels, maximum and minimum fuel-air ratios for burner stability and the rate and amplitude limits of all control variables (Reference 7). These constraints must be observed both in steady state and in transient modes. In addition to these constraints there are certain performance requirements such as providing correct steady state thrust and airflow levels and transient thrust response times. This set of constraints and requirements is independent of the method used to design the control. Although implementation as a controller may be impractical, the optimal control law provides insight useful in designing a more easily implementable suboptimal controller.

A special class of optimal control theory is the linear quadratic regulator (LQR) problem. For the LQR problem applied to a turbine engine, the optimal control law is a linear time-invariant function of

35

the system states. For the general system described by the linear state equations; (Reference ;

$$\dot{\bar{x}}(t) = \bar{A}(t)\bar{x}(t) + \bar{B}(t)\bar{u}(t) \tag{14}$$

The performance index (PI) to be minimized is;

$$PI = \tfrac{1}{2}\,\bar{x}^T(t_f)\bar{H}\bar{x}(t_f) + \tfrac{1}{2}\!\int_{t_0}^{t_f} [\bar{x}^T(t)\bar{Q}(t)\bar{x}(t) + \bar{u}(t)\bar{R}(t)\bar{u}(t)]dt \tag{15}$$

where: t_f = final time and is fixed

$\bar{H}$ and $\bar{Q}$ are real symmetric positive semi-definite matrices

$\bar{R}$ is real symmetric positive definite matrix

It is assumed that the states and controls are not bounded. The physical significance attached to the performance index is: It is desired to maintain the state vector, $\bar{x}$, close to the origin without an excessive expenditure of control, $\bar{u}$, effort.

For the situation wherein the process is to be controlled for an infinite duration, $t_f \rightarrow \infty$, it can be shown (Reference 11) that if the plant is completely controllable and $\bar{H} = 0$ than $\bar{A}$, $\bar{B}$, $\bar{R}$, and $\bar{Q}$ are constant matrices. Equations 14 and 15 then become;

$$\dot{\bar{x}}(t) = \bar{A}\bar{x}(t) + \bar{B}\bar{u}(t) \tag{16}$$

$$PI = \tfrac{1}{2}\!\int_0^\infty [\bar{x}^T(t)\bar{Q}\bar{x}(t) + \bar{u}^T(t)\bar{R}\bar{u}(t)]dt \tag{17}$$

The optimal control law for this case is derived using the Hamiltonian (Reference 11);

$$\bar{u}^*(t) = -\bar{R}^{-1}\bar{B}^T\bar{K}\bar{x}(t) \tag{18}$$

or

$$\bar{u}^*(t) = \bar{F}\bar{x}(t)$$

where $\bar{K}$ is obtained by solving the nonlinear Ricatti equation;

$$0 = -\bar{K}\bar{A} - \bar{A}^T\bar{K} - \bar{Q} + \bar{K}\bar{B}\bar{R}^{-1}\bar{B}^T\bar{K} \tag{19}$$

Before proceeding with the solution of the matrix Ricatti equation

36

It is necessary to rewrite Equations 16 and 17. Recalling the discussion on the linearization procedure, $\bar{x}$ and $\bar{u}$ were actually normalized deltas. For example if x_1 was fan speed, NI, then the linearization would have used $\Delta NI = (NI_{ss} - NI_p)/NI_n.$ Where NI_{ss} is fan speed at steady state, NI_p is perturbed fan speed from steady state and NI_n is the fan speed at PLA = 83 used to normalize. Therefore, Equation 16 should be;

$$(\Delta \dot{\bar{x}}(t)) = \bar{A}(\Delta \bar{x}(t)) + \bar{B}(\Delta \bar{u}(t))$$

To simplify the derivations that follow, the Δ's, t's and overlines will be dropped.

Next, recall that the linear system is described by:

$$\dot{x} = Ax + Bu \tag{20}$$

$$y = Cx + Du \tag{21}$$

let $X = \left| \dfrac{x}{u} \right|$ and $U = \dot{u}$

then $\dot{X} = \left| \begin{array}{c|c} A & B \\ \hline 0 & 0 \end{array} \right| X \cdot + \left| \begin{array}{c} 0 \\ \hline I \end{array} \right| U$

or

$$\dot{X} = A'X + B'U \tag{22}$$

let $Y = \left| \begin{array}{c} y \\ \hline x \\ \hline u \\ \hline \dot{y}_2 \end{array} \right| = \left| \begin{array}{c} y \\ \hline X \\ \hline \dot{y}_2 \end{array} \right|$ where $\dot{y}_2$ is the rate of change of y_2 in Table 2 and calculated according to the following formula;

$$\dot{y}_2 = \sum_{i=1}^{n} C_{2,i} \left[\sum_{j=1}^{n} A_{i,j} x_j + \sum_{j=1}^{m} B_{i,j} u_j \right] + \sum_{i=1}^{m} D_{2,i} U_i \tag{23}$$

then $Y = \left| \begin{array}{c|c} C & D \\ \hline I & 0 \\ \hline 0 & I \\ \hline C_2 A & C_2 B \end{array} \right| X + \left| \begin{array}{c} 0 \\ \hline 0 \\ \hline 0 \\ \hline D_2 \end{array} \right| U$

$$Y = C'X + D'U \tag{24}$$

37

The parameters of X and Y are presented in Table 7 for the VCE model. The redefined state vector now includes the original states and the control input variables. The redefined output vector includes the original output variables plus the redefined state vector and the time derivative of turbine inlet temperature. The control vector was redefined to be the rate of change for the control inputs. A FORTRAN program that automatically transforms the original A, B, C and D matrices into the form of Equations 22 and 24 was developed.

The purpose of these redefinitions was to allow the performance index, Equation 17, to be rewritten to allow the designer direct weighting of the state, output, control, and control rate variables. This is accomplished by adjusting the weighting matrices, Q and R in Equation 17. Adjusting the relative weights alters the solution of the minimization such that the more heavily weighted terms are driven to zero more rapidly than the lightly weighted terms.

The desired form for the performance index is;

$$PI = \frac{1}{2}\int_0^\infty [Y^TQY + U^TRU]dt \qquad (25)$$

and the optimal control law is;

$$U^* = -R^{-1}B^TKX \qquad (26)$$

This is no longer in the LQR format. Equation 25 is transformed by substituting for Y with Equation 24;

$$Y^TQY = [C'X + D'U]^TQ[C'X + D'U]$$

this is equivalent to;

$$Y^TQY = [C'X]^TQ[C'X] + [D'U]^TQ[D'U] + [C'X]^TQ[D'U] + [D'U]^TQ[C'X]$$

which reduces to;

$$Y^TQY = X^TC'^TQC'X + U^TD'^TQD'U + X^TC'^TQD'U + U^TD'^TQC'X$$

38

TABLE 7

REDEFINED STATE, INPUT, AND OUTPUT VECTORS

State Vector

X_1 = fan physical speed (N1)

X_2 = compressor physical speed (N2)

X_3 = afterburner volume total pressure (PT7)

X_4 = fan duct volume total pressure (PT6c)

X_5 = core exhaust nozzle area (AJC)

X_6 = fan inlet guide vane angle (CIVV)

X_7 = compressor stator vane angle (RCVV)

X_8 = main burner fuel flow (WF)

X_9 = fan duct exhaust nozzle area (AJD)

X_{10} = high turbine nozzle position (HTVPOS)

X_{11} = fan turbine nozzle position (FTVPOS)

Input Vector

U_1 = time derivative of core exhaust nozzle area (AJC)

U_2 = " " " fan inlet guide vane angle (CIVV)

U_3 = " " " compressor stator vane angle (RCVV)

U_4 = " " " main burner fuel flow (WF)

U_5 = " " " fan duct exhaust nozzle area (AJD)

U_6 = " " " high turbine nozzle position (HTVPOS)

U_7 = " " " fan turbine nozzle position (FTVPOS)

TABLE 7 (concluded)

Output Vector

Y_1 = net thrust (FN)

Y_2 = gas temperature at inlet to high pressure turbine (TT4M)

Y_3 = airflow through fan (WFAN)

Y_4 = fan surge margin (SMAF)

Y_5 = compressor surge margin (SMHC)

Y_6 = fan physical speed (N1)

Y_7 = compressor physical speed (N2)

Y_8 = afterburner volume total pressure (PT7)

Y_9 = fan duct volume total pressure (PT6c)

Y_{10} = core exhaust nozzle area (AJC)

Y_{11} = fan inlet guide vane angle (IGV)

Y_{12} = compressor stator vane angle (RCVV)

Y_{13} = main burner fuel flow (WF)

Y_{14} = fan duct exhaust nozzle area (AJD)

Y_{15} = high turbine nozzle position (HTVPOS)

Y_{16} = fan turbine nozzle position (FTVPOS)

Y_{17} = time derivative of gas total temperature at inlet to high turbine (TT4M)

let; $Q_1 = C'^T Q C'$ $\qquad$ $Q_3 = D'^T Q C' = Q_2^T$

$\qquad$ $Q_2 = C'^T Q D'$ $\qquad$ $Q_4 = D'^T Q D'$

then; $Y^T Q Y = [X^T, U^T] \begin{vmatrix} Q_1 & Q_2 \\ Q_2^T & Q_4 \end{vmatrix} \begin{vmatrix} X \\ U \end{vmatrix}$

and Equation 25 becomes;

$$PI = \tfrac{1}{2}\int_0^\infty [X^T, U^T] \begin{vmatrix} Q_1 & Q_2 \\ Q_2^T & Q_4+R \end{vmatrix} \begin{vmatrix} X \\ U \end{vmatrix} dt \tag{27}$$

According to Reference 14 (pg.157) Equation 27 is equivalent to;

$$PI = \tfrac{1}{2}\int_0^\infty [X^T, U^T] \begin{vmatrix} Q_1 - Q_2(Q_4+R)^{-1}Q_2^T & 0 \\ 0 & Q_4+R \end{vmatrix} \begin{vmatrix} X \\ U \end{vmatrix} dt \tag{28}$$

By letting; $R' = Q_4 + R$ and $Q' = Q_1 - Q_2 R'^{-1} Q_2^T$ Equation 28 reduces to;

$$PI = \tfrac{1}{2}\int_0^\infty [X^T Q' X + U^T R' U] dt \tag{29}$$

The optimal control law is given by;

$$U^* = R'^{-1}(Q_2^T + B'^T K)X \tag{30}$$

$\qquad$ or

$$U^* = F'X \quad \text{where; } F' = R'^{-1}(Q_2^T + B'^T K)$$

Where K is obtained by solving;

$$0 = -K(A'-BR'^{-1}Q_2^T) - (A'-B'R'^{-1}Q_2^T)^T K + KB'R'^{-1}B'^T K - (Q_1 - Q_2 R'^{-1}Q_2^T)$$

which reduces to;

$$0 = -KA' - A'^T K + KB'R'^{-1}Q_2^T - Q'$$

In summary the important equations for the quadratic regulator problem as used in this report are;

$$\dot{X} = A'X + B'U \tag{22}$$

$$Y = C'X + D'U \tag{24}$$

$$PI = \tfrac{1}{2}\int_0^\infty [X^T Q' X + U^T R' U] dt \tag{29}$$

$$U^* = R'^{-1}(Q_2^T + B'^T K)X = F'X \tag{30}$$

$$0 = -KA' - A'^T K + KB'R'^{-1}Q_2^T - Q' \tag{31}$$

41

4. INTERACTIVE RICATTI EQUATION SOLVER

A FORTRAN program that solves the Ricatti equation and outputs the feedback gain matrix of Equation 30 was developed from a program used in Reference 6. The linear matrix subroutines are from Reference 13. The program was written for a CDC 6600 computer to be operated interactively using a Tektronix 4014-1 interactive graphics unit. The user must supply a set of A, B, C, and D matrices from Equations 22 and 24, a set of state initial conditions, X, and a set of values for the diagonal matrices Q and R. With this information the program solves for K in Equation 31 and calculates the feedback gain matrix which is displayed and optionally punched out for use in a controller on the nonlinear transient simulation. Additionally the program displays on-line, transient responses of all the output variables in Table 7.

The optimal control law of Equation 30 is optimal only for the particular set of Q and R matrices input to the program and within the linear range of the A, B, C, and D matrices. There is no direct method of determing the "correct" values of Q and R for a particular set of imposed control rate limits and constraints. The process of selecting the set of values for Q and R that results in the desired transient response is an interactive process. This program and the interactive graphics allows the control designer to define the performance index and calculate the feedback gains for the transient response he desires in one sitting. It also gives him the capability to experiment with various performance index weightings and view the transient response of the output variables immediately. He can then ascertain the change to the feedback gain matrix

As an example, for the linear model at PLA = 60 (Table 6), the Q and R matrix values in Table 8, case 1, were finally selected to provide the "best" transient response. The transient response as seen on-line on the graphics unit is presented in Figure 8, Case 1. The transient is for a step change in PLA from 60 to 63. The output parameters displayed have been nondimensionalized and scaled. In this particular PLA operating range (CMVT) it is desired to hold the fan and compressor speed and pressure ratios constant, while fuel flow is added to increase turbine temperature and thrust. To accomplish this, large Q matrix weightings were given to the N1, N2, and WF errors with an order of magnitude less weighting to the FN, TT4M, WFAN, CIVV, and RCVV errors. Heavy weights were given to the CIVV, RCVV, and AJD rates of movements in the R matrix. This set of Q and R matrix values is one possible performance index (PI) which gives one particular set of feedback gains. As a comparison, Case 2 shows the transient response for the PI where all the output and control parameters were weighted equally. Transient response is very sluggish but N1 and N2 remain constant. Case 3 shows the transient response for the PI where very fast thrust response is desired but no other restraints placed on the other parameters. The thrust response for this case is extremely fast but a very large TT4M overshoot occurs which is very damaging to the turbine. N1 and N2 move a considerable amount from their respective CMVT values. Although optimal control techniques do not provide a direct method to calculate the "best" transient response, the interactive Ricatti equation solver provides the control designer with an excellent design tool that quickly calculates a set of feedback gains for a multivariable controller.

TABLE 8

PERFORMANCE INDEX (FI) WEIGHTINGS (PLA=60)

Q Diagonal

Weigthings for Output Variables from Table 7

Case 1

Y_1	Y_2	Y_3	Y_4	Y_5	Y_6	Y_7
10000.	10000.	10000.	1.	1.	500000.	100000.

Y_8	Y_9	Y_{10}	Y_{11}	Y_{12}	Y_{13}	Y_{14}
1.	1.	1.	10000.	10000.	200000.	1000.

Y_{15}	Y_{16}	Y_{17}
1000.	1000.	1.

Case 2

Y_1	Y_2	Y_3	Y_4	Y_5	Y_6	Y_7
1.	1.	1.	1.	1.	1.	1.

Y_8	Y_9	Y_{10}	Y_{11}	Y_{12}	Y_{13}	Y_{14}
1.	1.	1.	1.	1.	1.	1.

Y_{15}	Y_{16}	Y_{17}
1.	1.	1.

Case 3

Y_1	Y_2	Y_3	Y_4	Y_5	Y_6	Y_7
1000000.	1.	1.	1.	1.	1.	1.

Y_8	Y_9	Y_{10}	Y_{11}	Y_{12}	Y_{13}	Y_{14}
1.	1.	1.	1.	1.	1.	1.

Y_{15}	Y_{16}	Y_{17}
1.	1.	1.

TABLE 8 (concluded)

R Diagonal

Weighting for Input Variables from Table 7

Case 1	U_1	U_2	U_3	U_4	U_5	U_6	U_7
	1.	1000.	1000.	1.	1000.	1.	1.

Case 2	U_1	U_2	U_3	U_4	U_5	U_6	U_7
	1.	1.	1.	1.	1.	1.	1.

Case 3	U_1	U_2	U_3	U_4	U_5	U_6	U_7
	1.	1.	1.	1.	1.	1.	1.
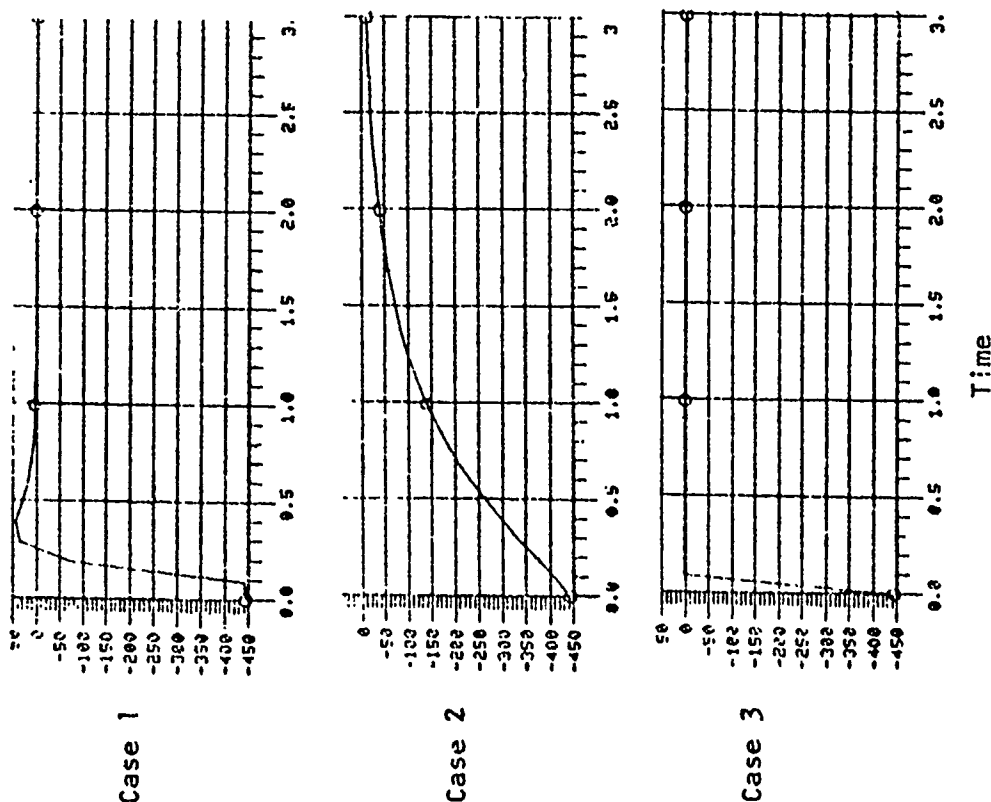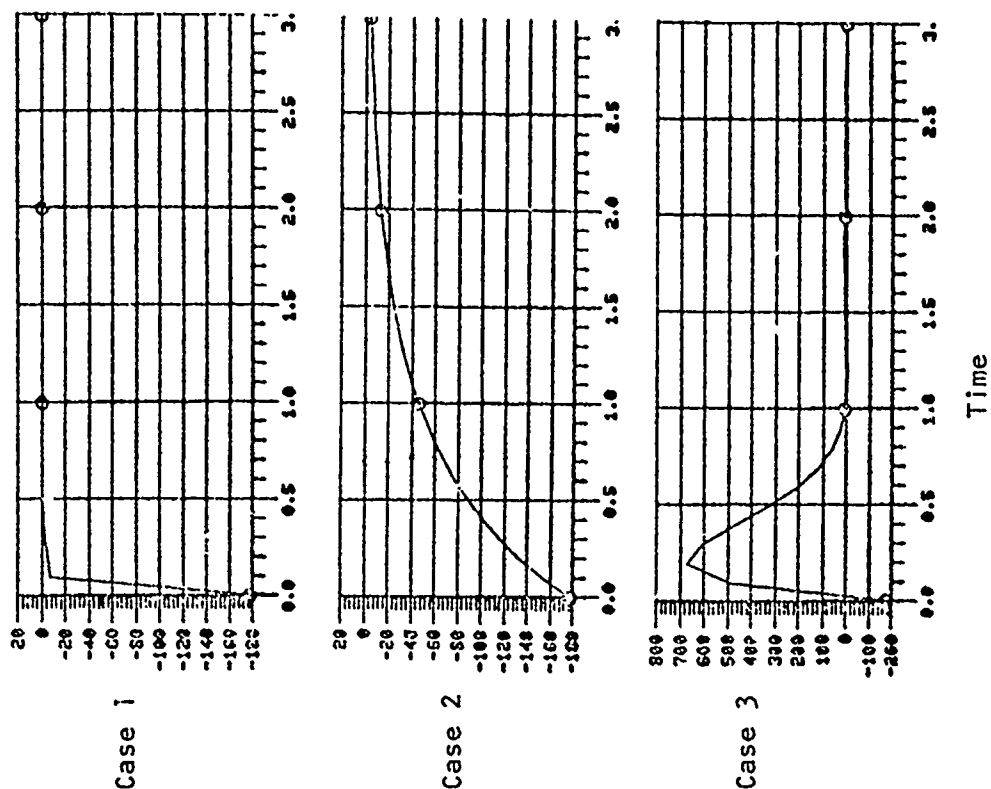
Figure 8. Transient Response for Various Performance Indexes (PI)
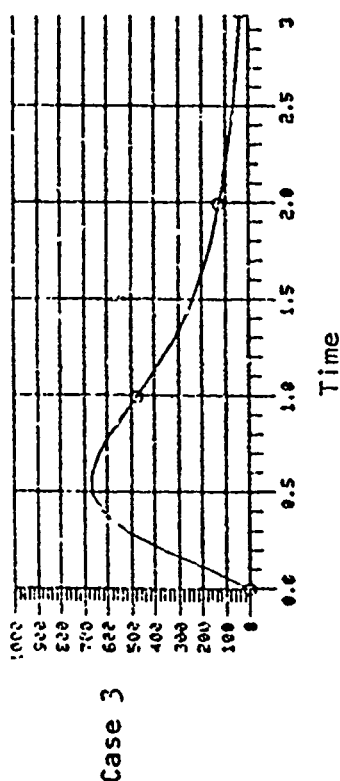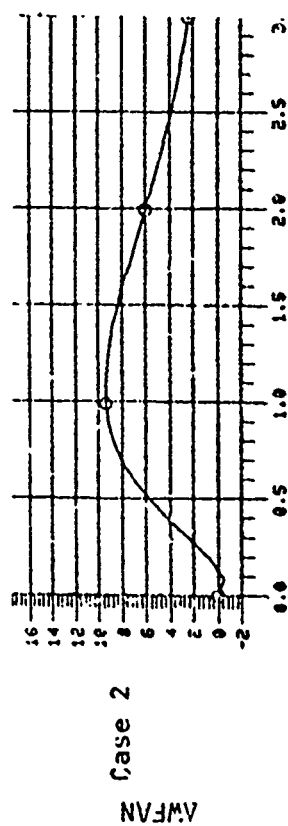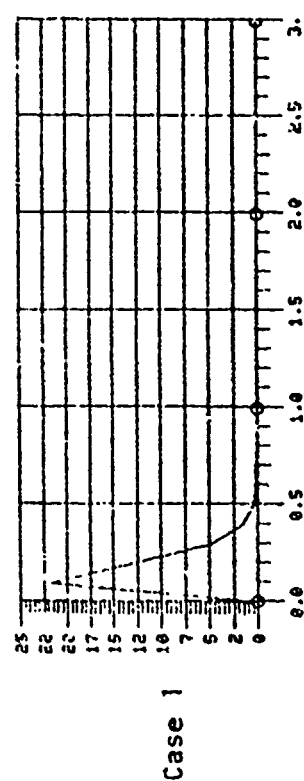
(100 units = 1.0% change of Intermediate value)

46

Figure 8. (continue)

47

Figure 8 (continue)

48

Case 1

Case 2

Case 3

ΔPT7

Case 1

Case 2

Case 3

ΔN2

Time

Time
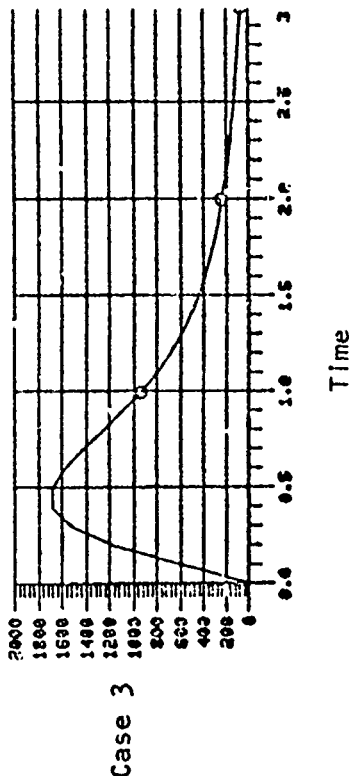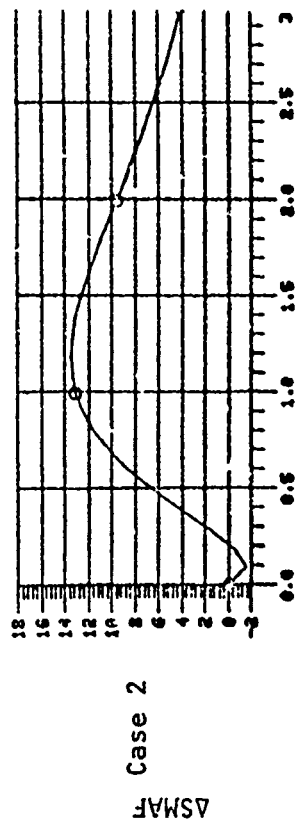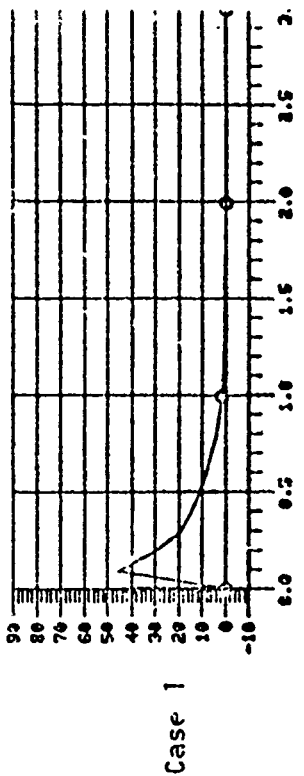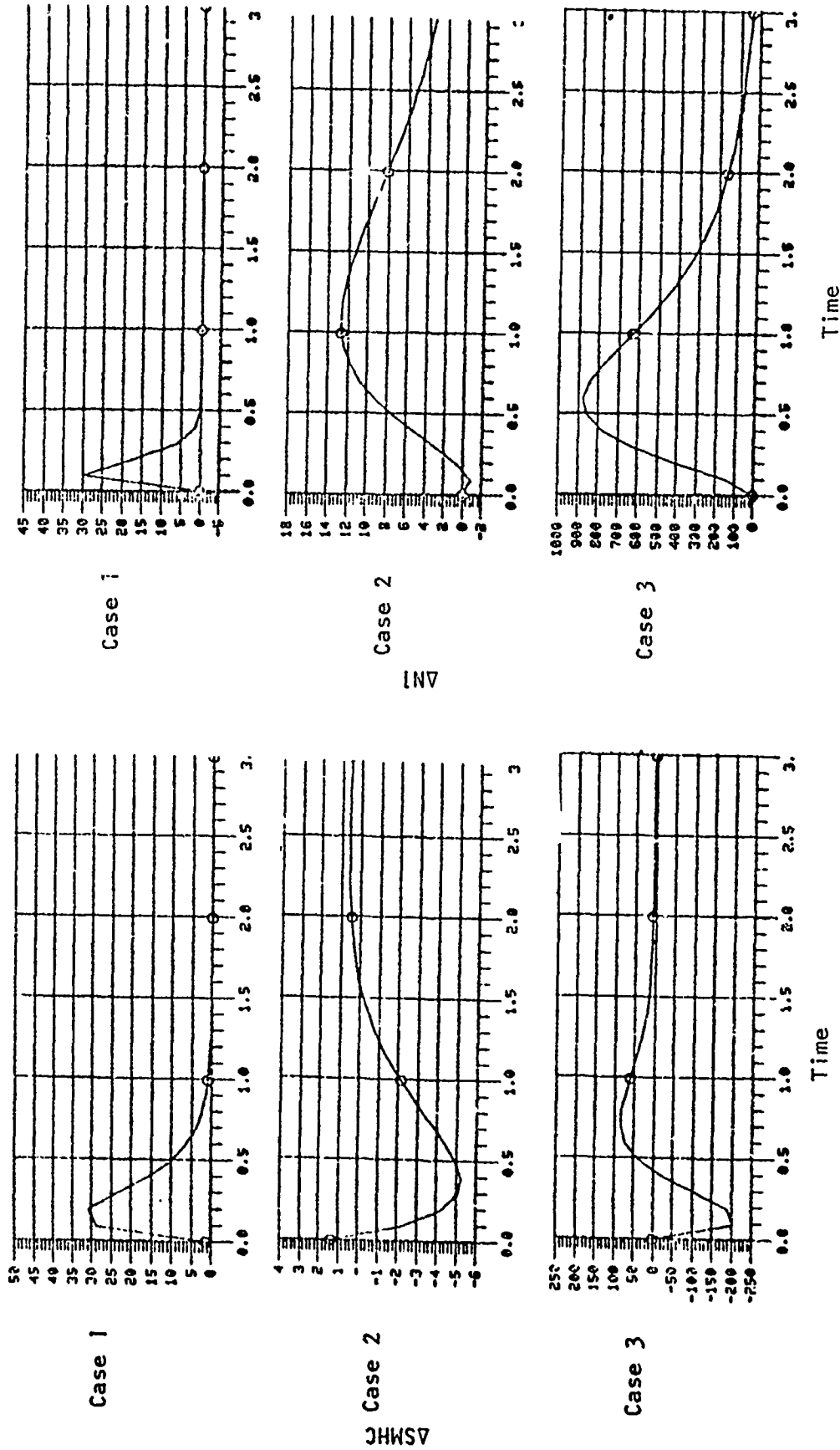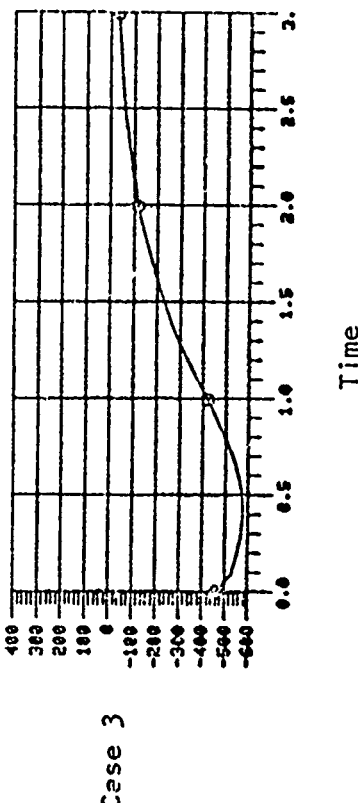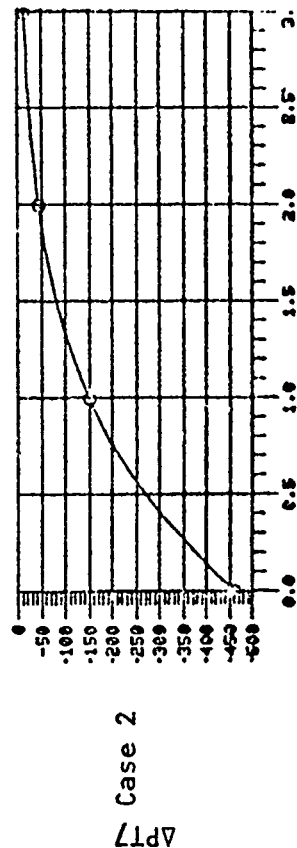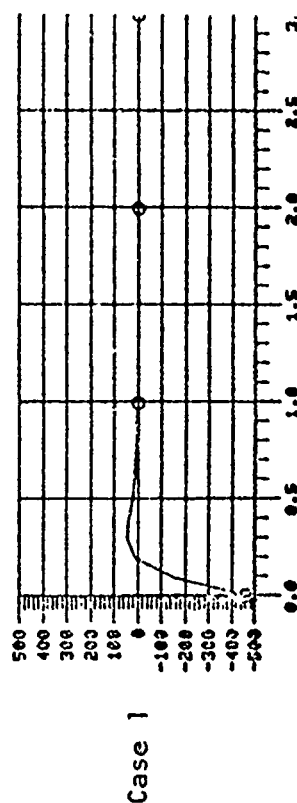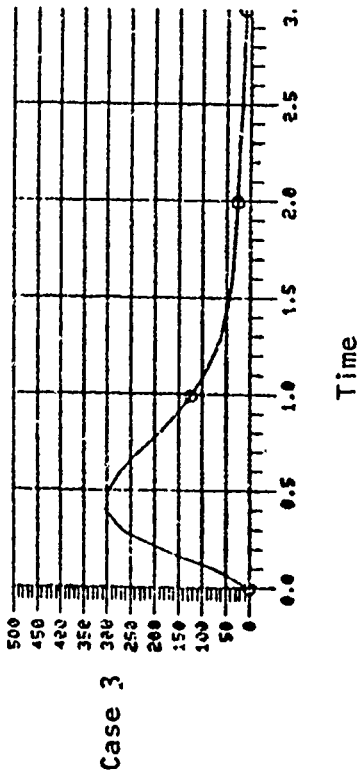
Figure 8 (continue)

Figure 8 (concluded)

5. OPTIMAL CONTROL LAW IMPLEMENTATION ON NONLINEAR DYNAMIC SIMULATION

Before discussing the nonlinear application aspects of the optima.
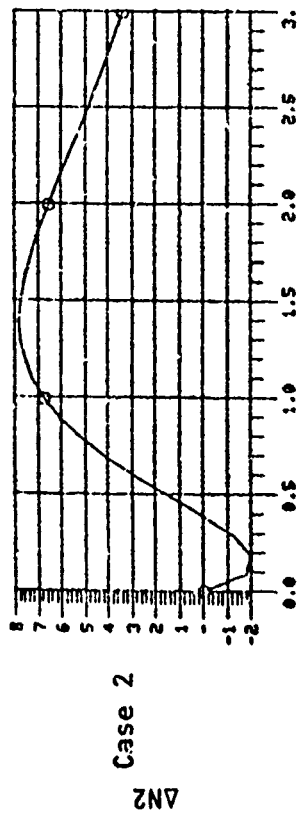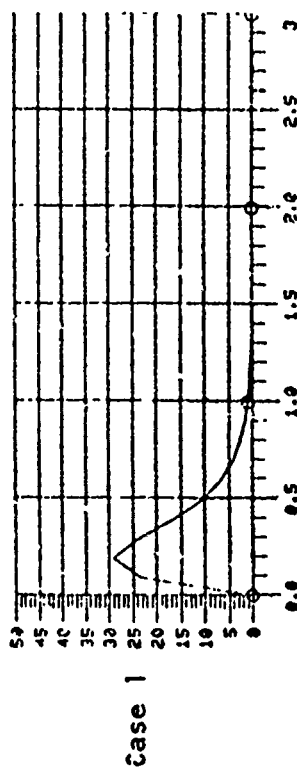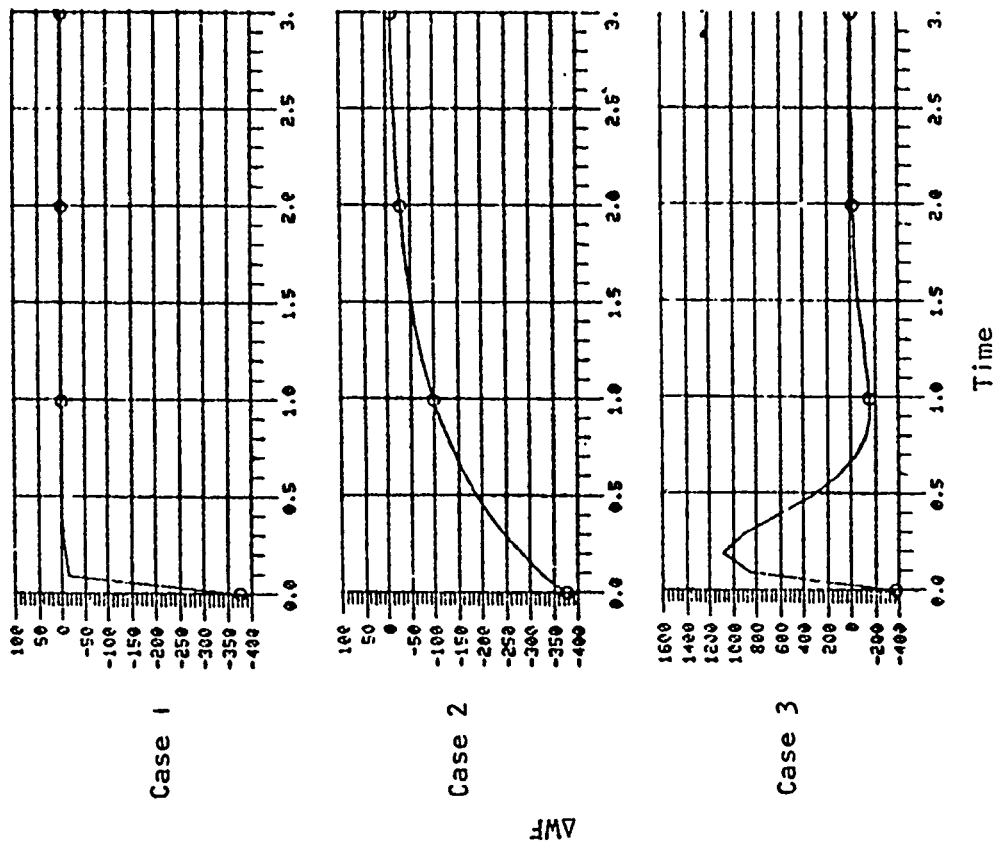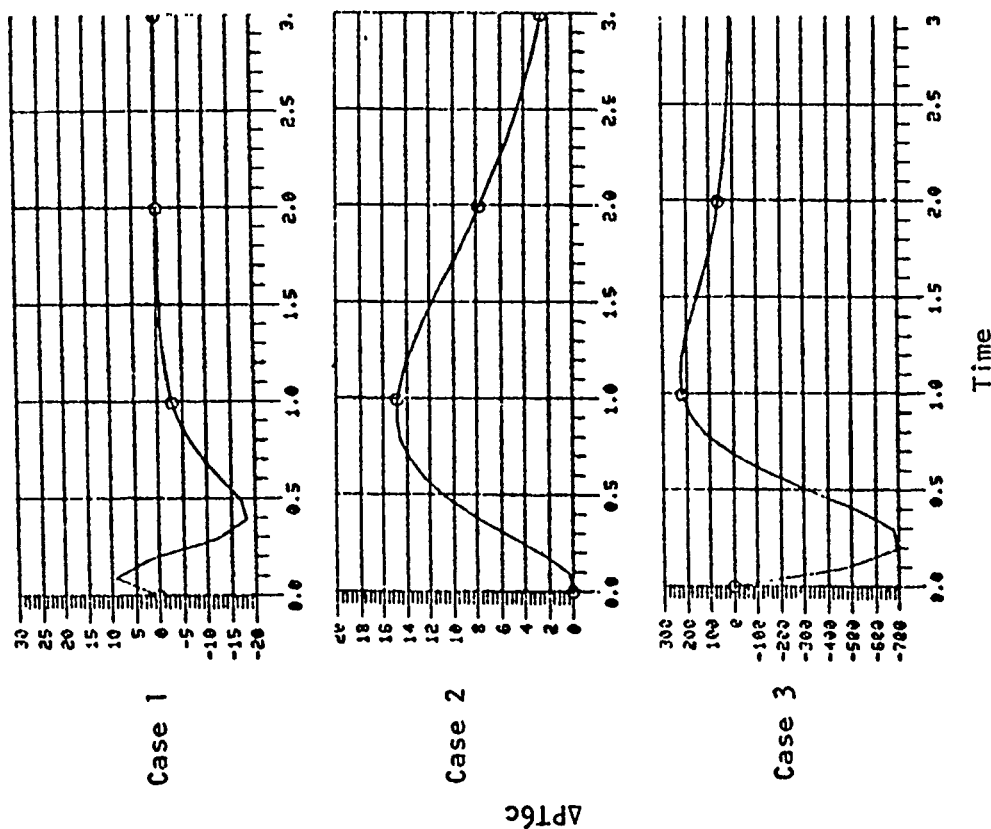control law, a summary is provided of the steps taken to derive the
optimal control law.

a. Develop nonlinear dynamic model

b. Derive steady state control schedules

c. Generate linear models (A, B, C, D matrices) at selected
   power settings

d. Reduce order of linear models

e. Transform A, B, C, and D matrices to the form of subsection 3

f. Calculate feedback gain matrices for small perturbation at
   each selected power settings using the reduced order models

A number of problems arise in adapting the optimal control law
of the last section to the nonlinear dynamic simulation. These are:

a. Feedback gains generated for small transients won't work for
   large transients

b. Control variable saturation

c. Power range of applicability for particular optimal control law

d. Transition from one set of feedback gains to another set

e. Steady state control

f. Control complexity

The linear models used for this study were calculated about various
power settings using small perturbations. The validity of a linear
model over a range of power settings has a direct bearing on the range
of applicability of the optimal control feedback gains. At the sea
level static condition, two linearizations were required to adequately
represent the VCE nonlinear model over the entire power range. Linear

51

models were initially calculated about five different power settings (PLA = 25, 35, 50, 60, 83). Recalling that the VCE operates in two modes, CMVT above PLA = 55 and non-CMVT below PLA = 55, an attempt was made to represent the entire power range with just two linear models. The obvious advantage of doing this is the reduction in the number of feedback gains that must be stored. The two linearizations selected were at PLA = 35 and 60. These linear models are presented in Table 5. The two linearizations were selected because their feedback gains provided what was considered to be adequate transient response over their respective non-CMVT and CMVT ranges. Obviously the optimal feedback gains will not be optimal over the entire operating range, thus resulting in a somewhat degraded transient response. This difference was not quantified.

Figure 9 shows a schematic of the regulator controller as implemented on the nonlinear transient simulation. All of the states, X, are fed back and an error calculated between the operating value and a reference value. The reference values are the steady state values of the control inputs and states as shown in Figure 5. The transformed state matrix, X, was schematically reduced to x and u to demonstrate that only the four states (N1, N2, PT7, PT6C) require measurement. The seven control inputs are calculated within the controller so that, assuming suitable positioning mechanisms, they do not require measurement.

The rate limited power level angle (PLAP) shown in Figure 9 was implemented to account for large rapid step changes in PLA. The optimal feedback gains were calculated for small transients (PLA = 60-63). For a set-point controller, the control input is proportional to the
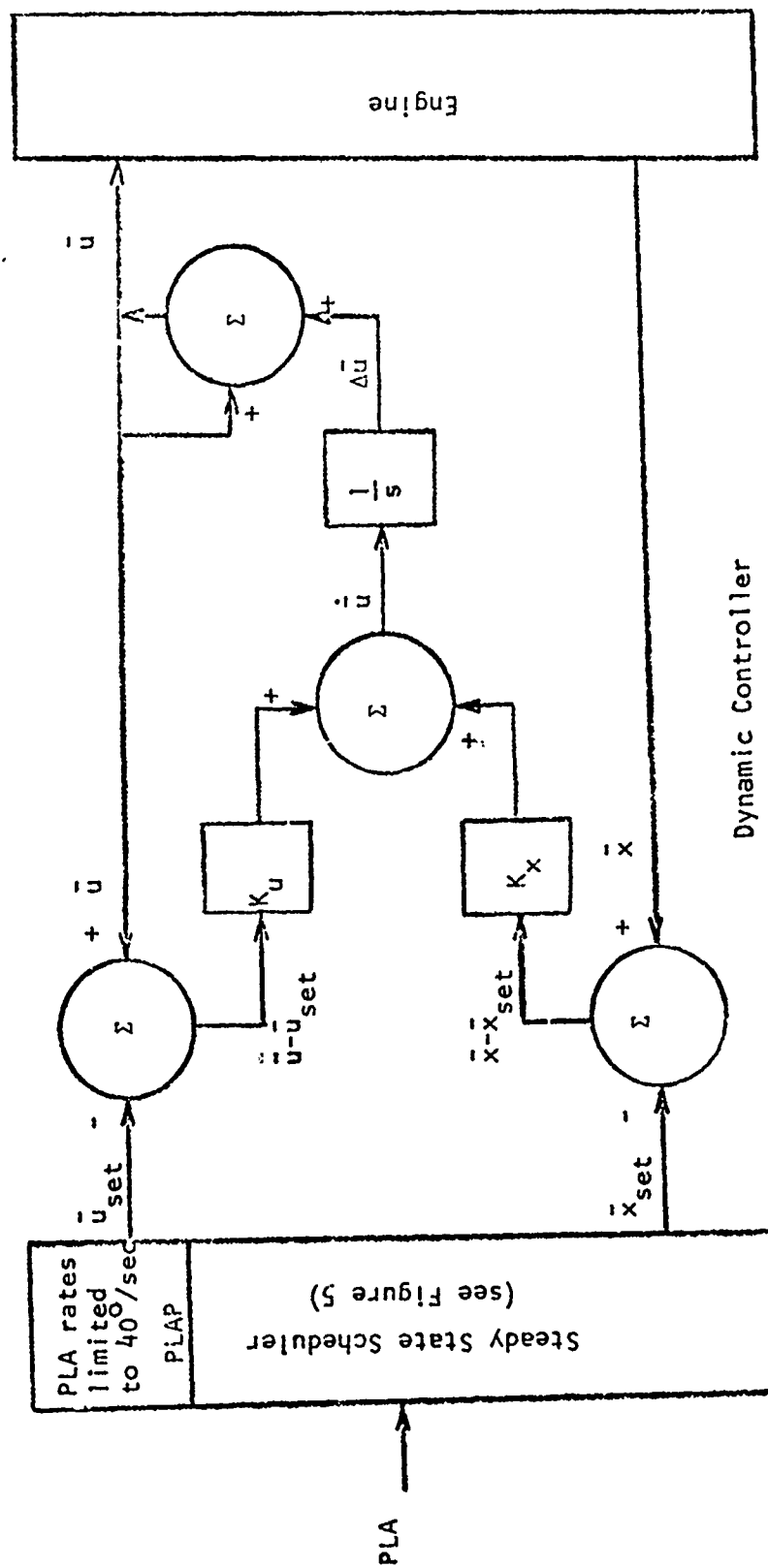
52

Figure 9. Schematic of Regulator Control

53

gain multiplied by the error signal. For small PLA changes, the difference between the state reference and the operating values is small and the small error signal multiplied by a given gain provides suitable performance. For large PLA changes, the given gain multiplied by a large error signal causes large excursions in the control inputs which can cause temperature overshoots and compressor stalls. PLA rate limiting provides a simplified means by which the error signal size is regulated by controlling rate of change of the state reference values. PLAP is allowed to vary at 40 degrees per second. This value was found to be the best compromise between the small and large transient responses. Other approaches to the error magnitude problem include the use of acceleration schedules on critical states (Reference 7) and scaling the gains as a function of actual fan rotor speed divided by the reference fan speed (Reference 6). All of these approaches result in the actual controller being to some degree, degraded from the optimal.

Another aspect of the large transient problem is the necessity to transition from one set of feedback gains to the other. The CMVT breakpoint occurs at PLA = 55. One set of feedback gains was derived for the below CMVT range and the other for the CMVT mode. A simple approach to transitioning would be to select a fan or compressor rotor speed at which the transition would occur. This approach was used in References 5 and 6. A result of using this approach is that discontinuities occur in the output and state variables. The approach used in this study was to set up a compressor speed range during which the two sets of feedback gains are gradually transitioned. This logic is shown schematically in Figure 10. The method is basically an averaging of

FB_h = Feedback gain matrix for CMVT range
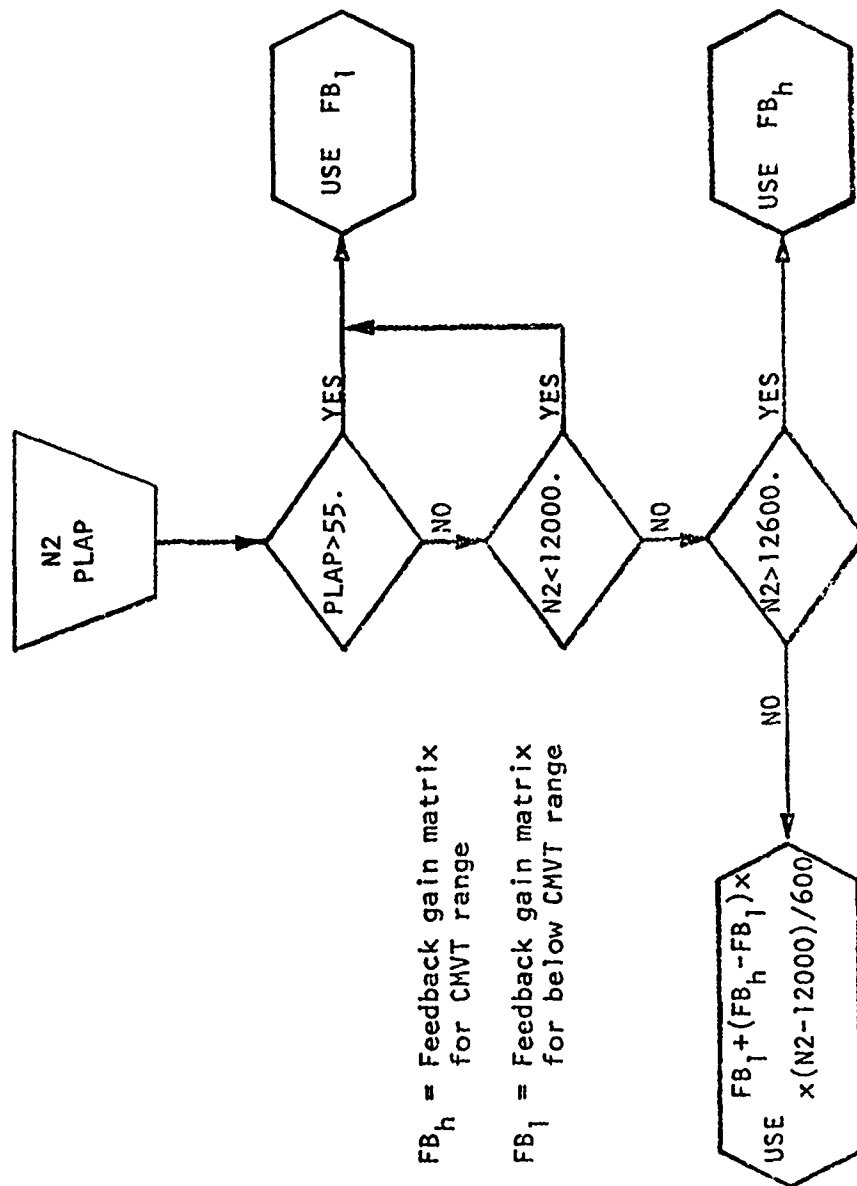
FB_l = Feedback gain matrix for below CMVT range

Figure 10. Feedback Gain Transitioning Logic

the feedback gains over a transition range of speeds and did an adequate job of reducing the discontinuity caused by the transition from one set of feedback gains to another during large transients.

Control variable saturation presented an additional suboptimal factor. The development of the optimal control law assumed that the control inputs were unconstrained. The actual inputs do have physical limits, such as minimum and maximum nozzle areas or vane movements. During a transient this is not a serious problem because the controller will eventually bring the control input off its limit. The controller is doing the best it can by staying on the limit as long as the optimal request is forcing the control in that direction.

When a steady state condition, as determined by lack of control variable movement, is reached after a transient, control variable saturation presents a fundamental problem. The saturated control variable is unable to move to zero out its own error, thus causing the other control variables to move off their desired steady state position, resulting in steady state errors. This problem was discussed in Reference 7. No general solution was found but a specific solution was stated. Some of the causes of this control saturation include inaccuracies in the scheduling and sensing of parameter, changes in component efficiences or installation effects such as customer bleeds. These effects were studied and are presented in the next section.

Steady state control is accomplished using the same feedback gains as used for the transients. No attempt was made to generate special steady state control logic such as maximum turbine inlet temperature limit or rotor speed schedules. The engine operating state is determined by the reference schedules, installation effects, ambient conditions,

and component efficiencies. Present day turbine engines require periodic adjustments (trim) to their steady state control schedules to account for component deterioration. These trims usually affect only the maximum (PLA = 83) operating condition by moving the control limits or schedules up or down. For the linear regulator controller, the reference schedules could be trimmed to accomplish the same effect. The other approach would be to allow the regulator controller to operate with whatever steady state errors that fall out and hope no physical limits are exceeded. Previous reports have not adequately addressed this problem. The next chapter will discuss this area for the specific operating range used in this report.

A final problem area with adapting the optimal control law concerns control complexity. By definition, linear regulator theory requires that all the state variables and control inputs must be fed back to have an optimal control. This requires a good deal of storage for the feedback gain matrices and computational effort. Various methods are available to reduce the number of feedback gain terms without significantly reducing the system response (References 7 and 13).

The straight forward approach is to compare the magnitudes of the normalized gains, eliminating all the gains less than a preselected magnitude, and reevaluating response to insure system response has not been significantly affected. As an example, for the feedback gain matrix of Table 9, CMVT mode, core exhaust nozzle area could be calculated considering only gain terms greater in absolute magnitude than 20. Instead of 11 feedback terms only four terms would be necessary. Beattie in Reference 7 reduced the number of gain terms for his case from 50 to 21 using this approach. A more rigorous technique was presented in

57

TABLE 9

FEEDBACK GAIN MATRICES

Below CMVT

	x_1	x_2	x_3	x_4	x_5	x_6	x_7	x_8	x_9	x_{10}	x_{11}
u_1	1.27	1.29	-.21	-.14	22.37	.00	-.09	.63	.05	-.01	.06
u_2	-.12	.05	.00	.01	.00	4.46	-.065	.03	.01	.00	-.00
u_3	-.39	.60	.05	.14	-.00	-.00	4.59	-.05	-.05	-.07	-.04
u_4	1.18	1.87	-.19	-.10	.01	.03	-.02	5.38	.10	.25	.00
u_5	4.56	18.0	-1.06	-7.42	.05	.65	-2.60	4.71	7.52	-.14	.14
u_6	2.53	-64.1	.34	.51	-.01	.09	-3.05	17.2	-.12	18.5	.44
u_7	10.9	-11.0	-1.40	-.99	.06	-.02	-2.19	.75	.14	.46	4.57

CMVT

	x_1	x_2	x_3	x_4	x_5	x_6	x_7	x_8	x_9	x_{10}	x_{11}
u_1	250.	199.	-77.	-7.35	35.2	17.1	-14.3	1.35	12.8	.39	3.59
u_2	.57	.37	-.24	-.04	.02	3.20	-.02	.00	-.00	.00	.01
u_3	-1.17	.22	.23	-.01	-.01	-.02	3.31	-.01	.03	.00	-.03
u_4	138.	73.1	-15.7	-1.13	1.08	2.15	-2.53	404.	.10	.31	1.52
u_5	-.93	.23	1.66	.29	.13	-.06	.34	-.00	3.53	.00	-.03
u_6	-10.1	46.8	-4.35	-2.54	.37	.51	3.21	-5.18	.36	31.9	-.59
u_7	460.	29.7	-70.0	.42	3.59	8.14	-26.5	1.81	-2.91	-.57	39.8

Reference 13 which analytically evaluates the importance of each gain

term on system response. This was done by evaluating the following

integral for each gain term eliminated;

$$PI = \int_0^\infty ([Y-Y^*]^T Q[Y-Y^*] + [U-U^*]^T R[U-U^*])dt$$

Where: Y^* = full output vector

Y = limited output vector

U^* = full control vector

U = limited control vector

Q = output weighting matrix

R = control weighting matrix

Although the reduction of feedback gain terms results in a further

deviation from the optimal control law, it is obvious that the linear

regulator theory and the feedback gain reduction methods provide a

systematic approach to determine the minimum number of gain terms

required and their values. It also provides a performance measure of

how nearly optimal the final controller is. Conventional control tech-

niques do not provide a systematic approach to determine the cross

coupled terms.

SECTION IV

NONLINEAR MODEL APPLICATION RESULTS

The previous chapter discussed the problem areas associated with adapting the optimal control law of Equation 30 to the nonlinear model. This chapter will discuss the results from the nonlinear adaptation. All results are for sea level static condition only, using the two sets of feedback gains given in Table 9. These two sets of feedback gains were derived for two unique performance indexes (PI) that were considered to provide the "best" transient response while operating within all the constraints. These constraints were the same (turbine temperature limits, stall margins etc.) that have to be observed independent of which design method is used to calculate the feedback gain terms. The purpose of this section is to present results when transient inputs are applied to the nonlinear model and also to discuss how well the control handles "real world" transient and steady state changes in the model, sensors, and actuators.

Figure 11 shows the transient response of the VCE nonlinear model using the controller of Figure 9. All of the output, state, and control variables are plotted. The transient is from idle thrust (PLA = 20) to maximum nonaugmented intermediate thrust (PLA = 83). Thrust (FN) reaches 95% of its intermediate value in about 2 seconds with no overshoot or steady state oscillation. Turbine-in temperature (TT4M) did not exceed its intermediate value which is critical to maintaining turbine life. The leveling off at 1 second is caused by the transition from the low feedback gain matrix to the high gain matrix. Fan airflow (WFAN), which is important for spillage drag as explained earlier, reaches steady state after only 1.25 seconds. Because thrust is a combination of airflow and pressure, this says that the first half of the

60

transient thrust increase is contributed almost entirely by airflow and fan duct pressure (PT6c) increase. Core exhaust pressure (PT7) remains almost constant the first second and then increases rapidly for the next second. As a comparison, Figure 16 (base case displayed later) shows the same transient for the original F100 nonlinear model. Thrust levels off at 93% at about 3.5 seconds but does not reach full thrust until about 5.75 seconds. Maximum airflow is not reached until about 2.75 seconds. The stall margins (SMAF and SMHC) are approximately the same for both models. Weinberg (Reference 6) using the original F100 nonlinear model and a multivariable control attained maximum thrust and airflow in about 3 seconds. Beattie (Reference 1) using a VCE model and conventional control design showed thrust and airflow transients of 5 seconds to attain maximum values. Using the same model but with a multivariable control, Beattie (Reference 7) showed a thrust response of 4 seconds for the idle to intermediate transient, but for a small transient similar to Figure 13, the transient response occurs in 0.25 seconds.

Figure 12 presents a deceleration from intermediate thrust to idle thrust. The time required to reduce thrust is an important control design consideration for air combat manuevers. Idle thrust is reached after about 2.5 seconds with no problem with stall margins. The only significant problem was caused by the fuel flow (WF) going too low and possibly causing a flameout. This could be overcome by putting a minimum fuel flow limit on the control. This would not affect the thrust response. Maximum and minimum limits were placed on some of the other control acutators. The dashed lines in Figure 5 show these limits.

Figure 13 shows a small transient in the CMVT range. In this range

61
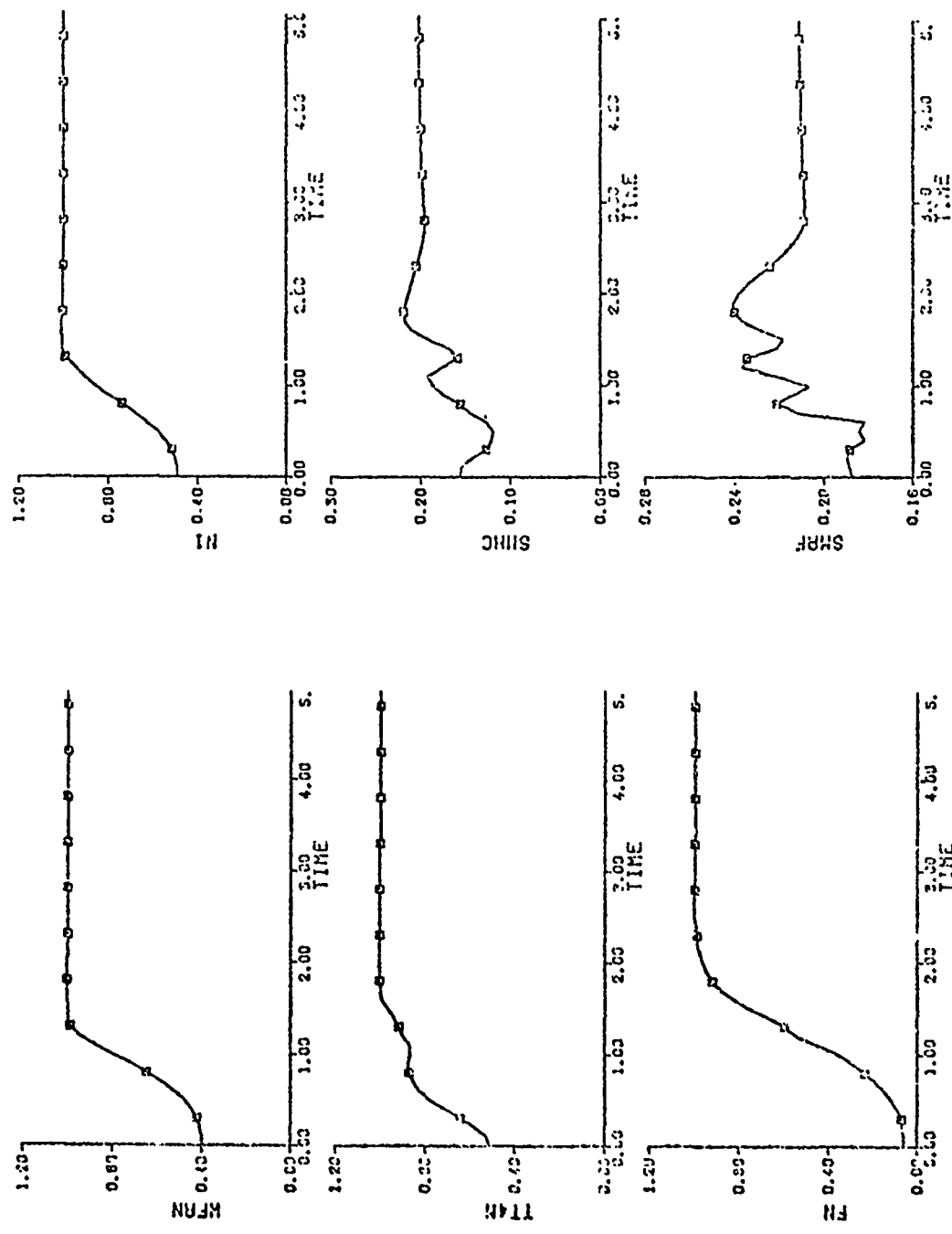
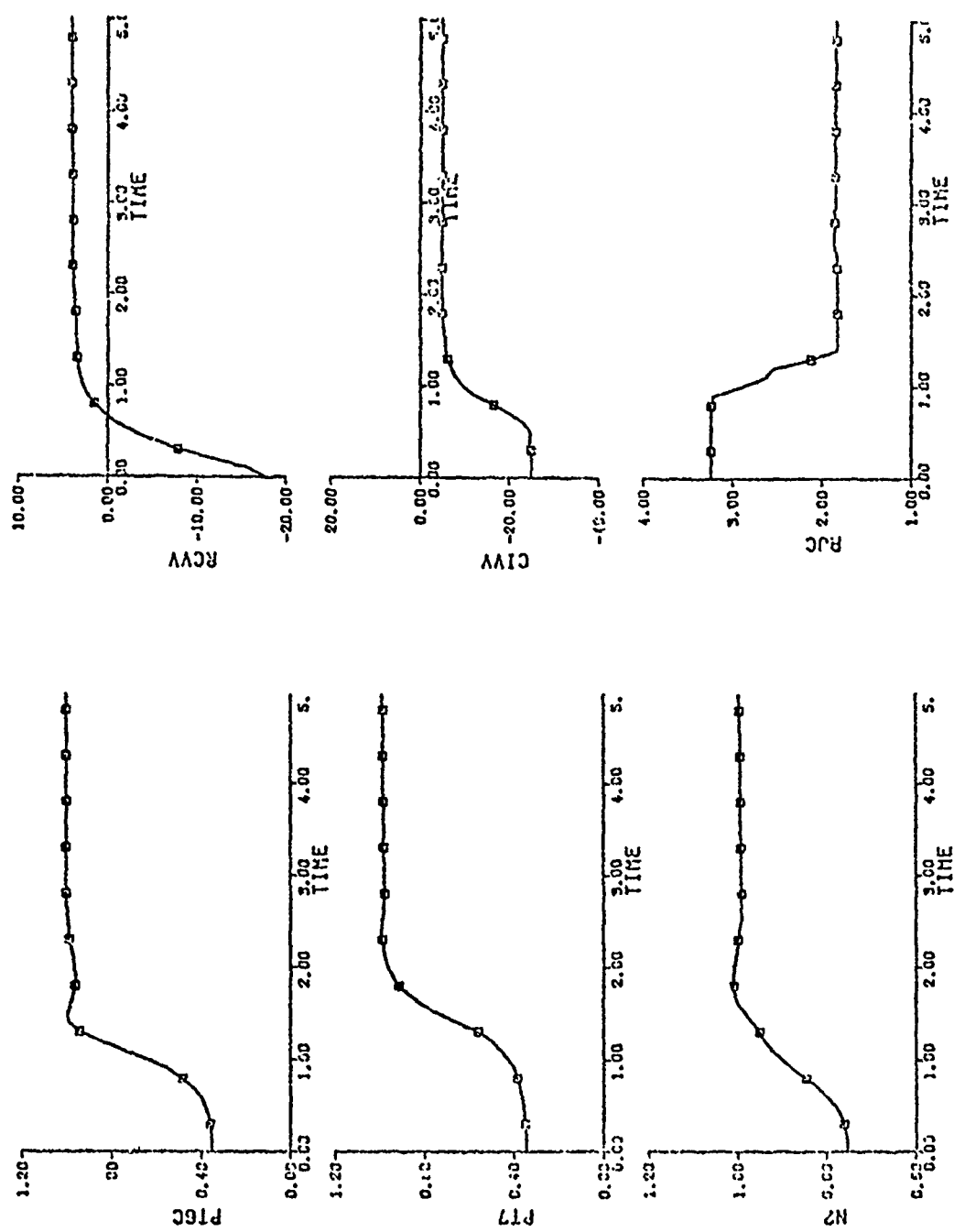Figure 11. Transient Response for VCE Nonlinear Model (PLA=20 to PLA=83)
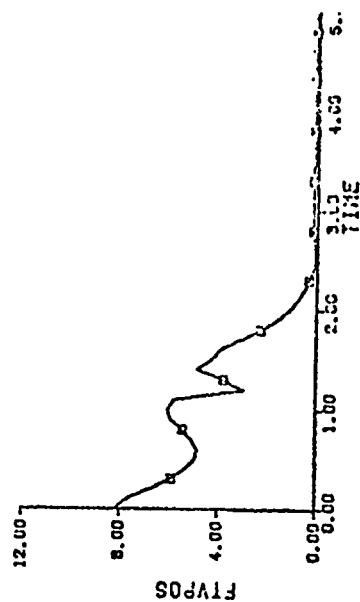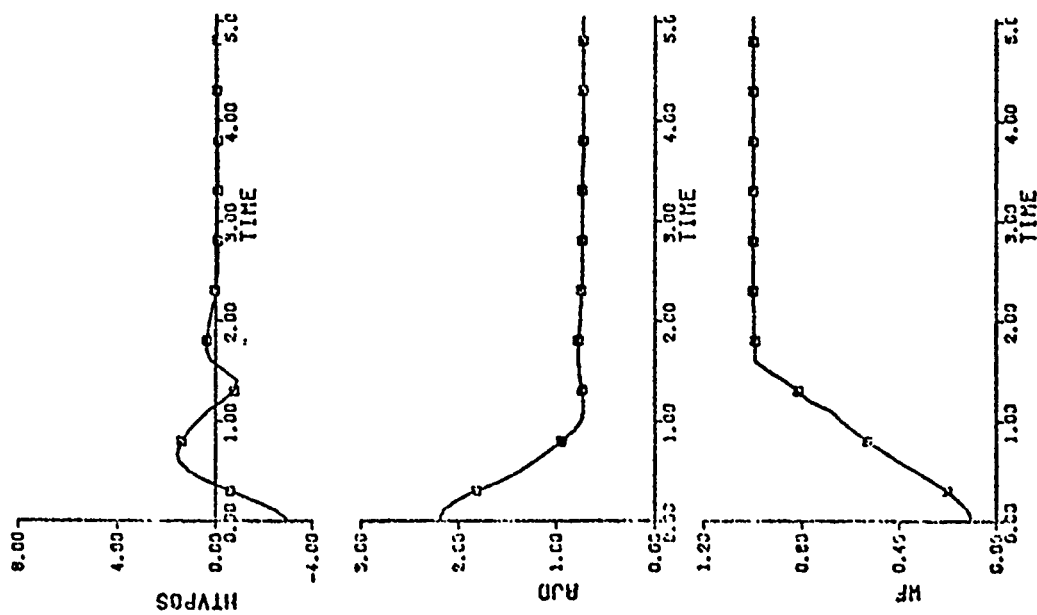
Figure 11. (continue)
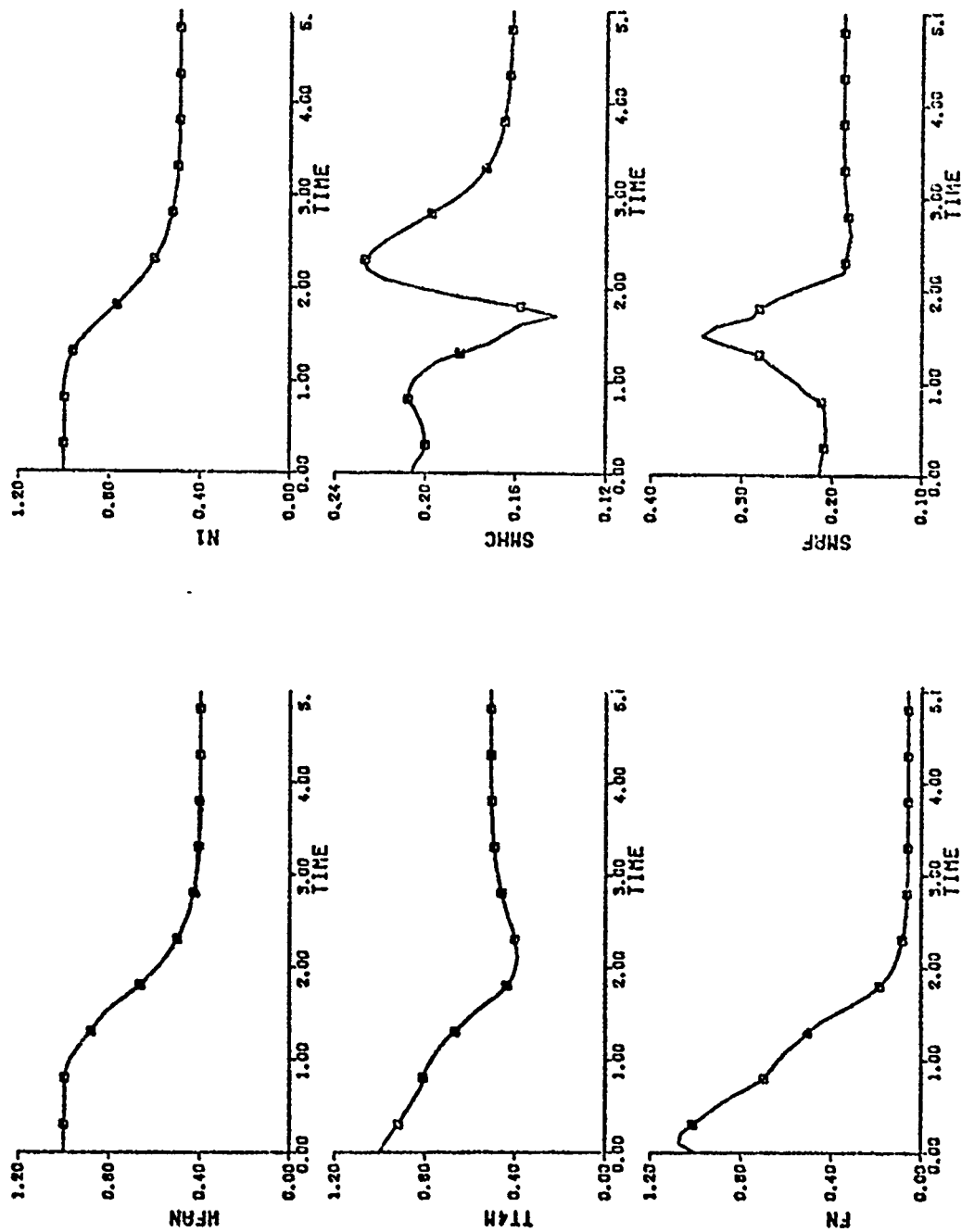
63

Figure 11. (concluded)

64

Figure 12. Transient Response for VCE Nonlinear Model (PLA=83 to PLA=20)
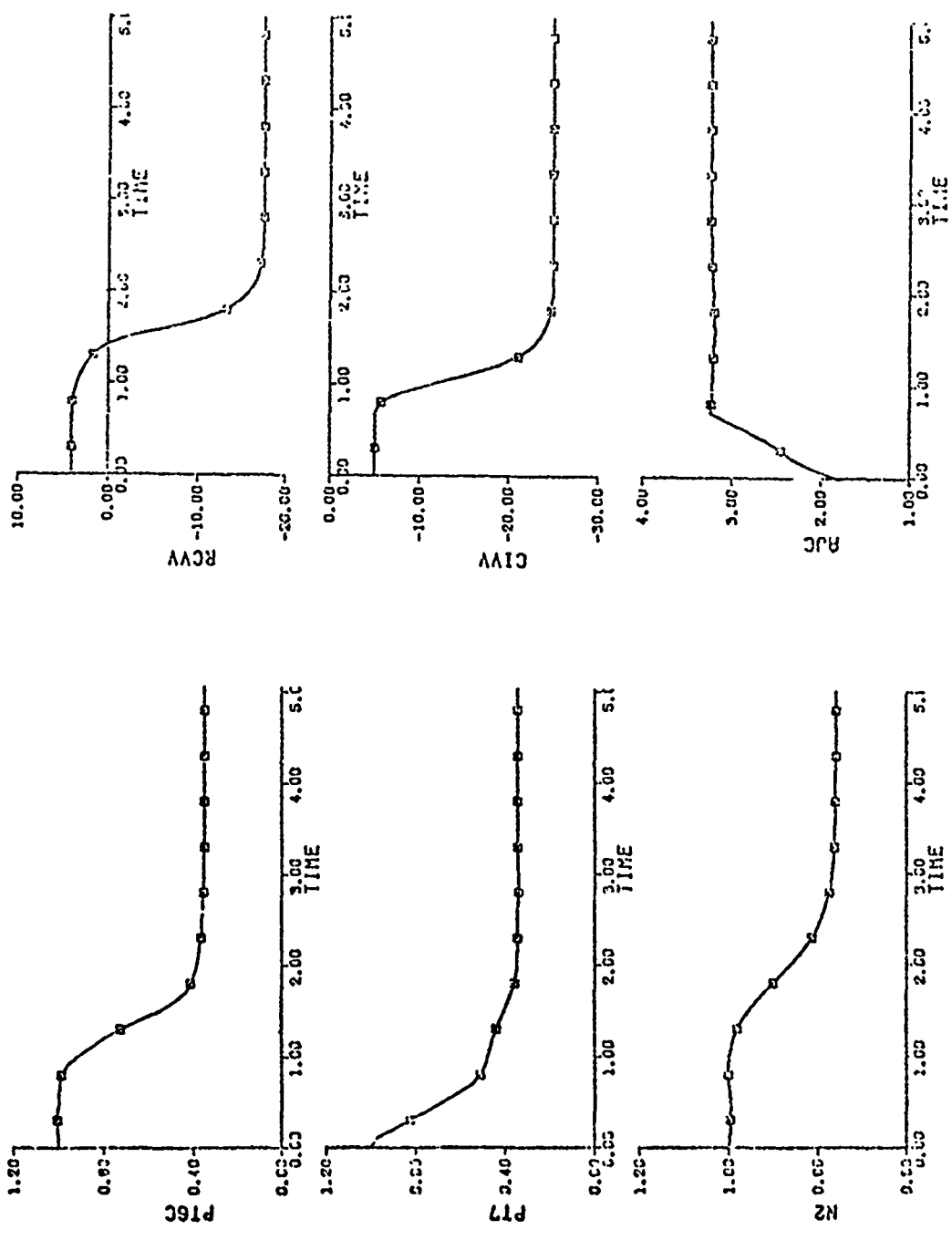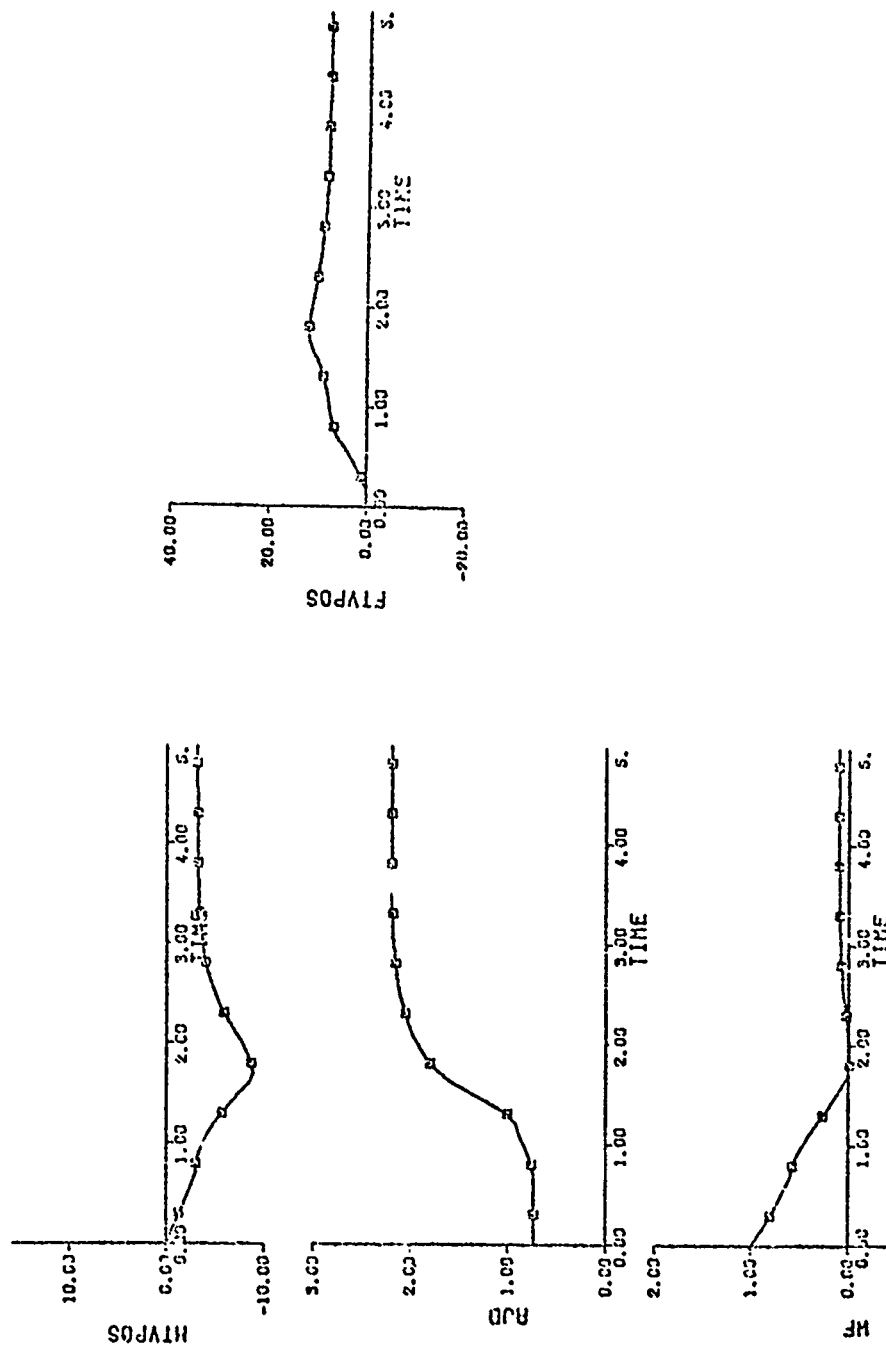
65

Figure 12. (continue)

Figure 12. (concluded)

67
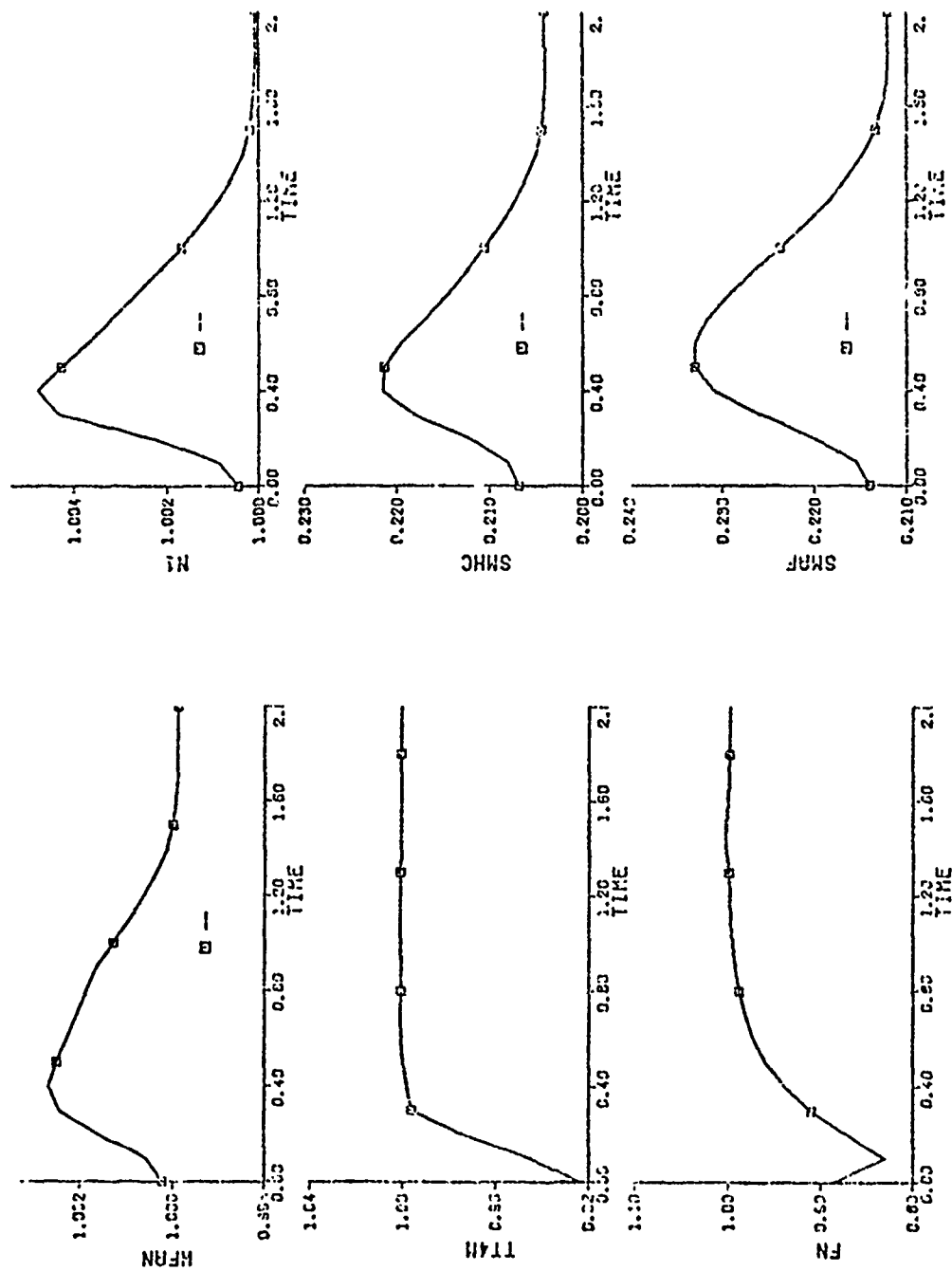
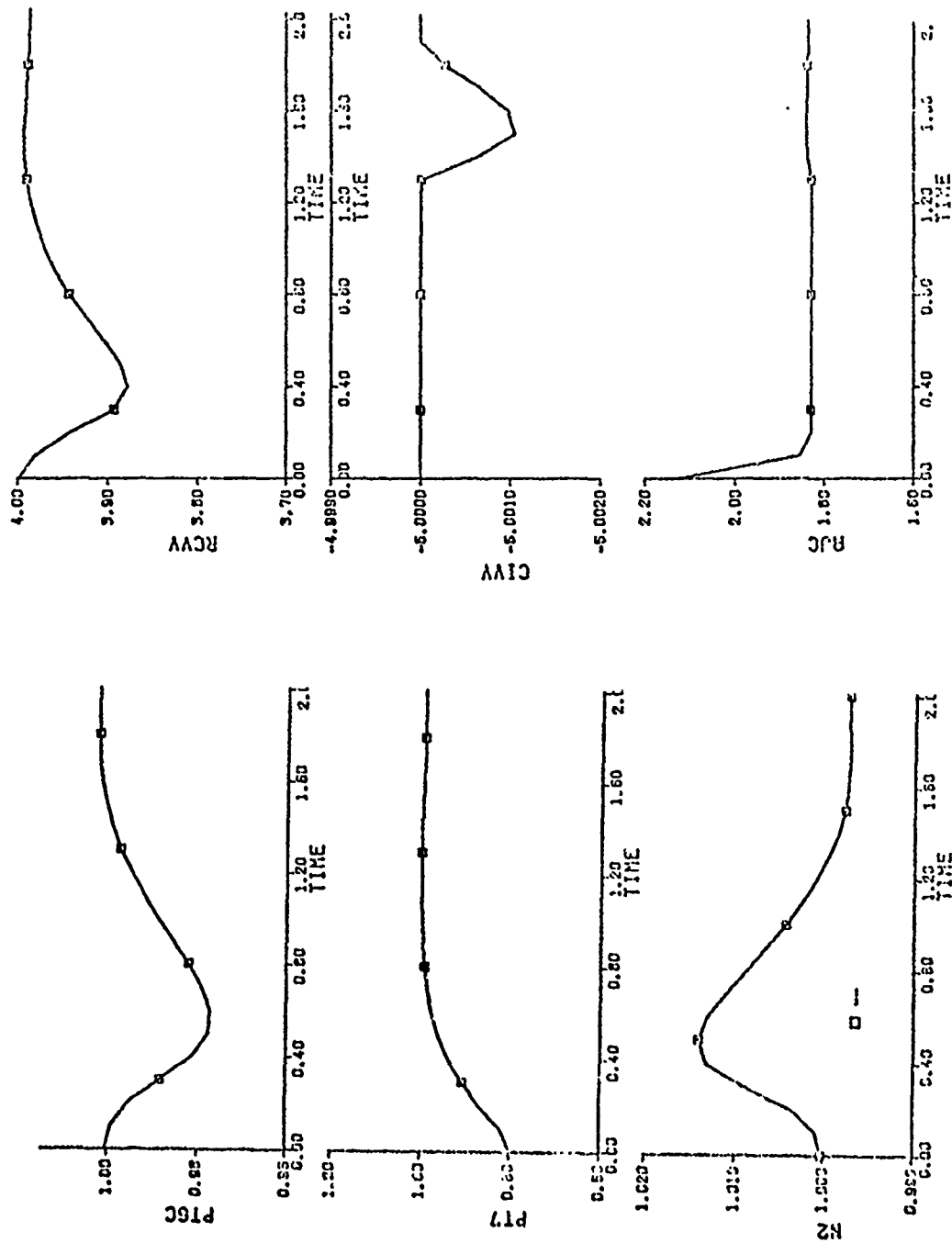Figure 13. Transient Response for VCE Nonlinear Model (PLA=73 to 83)
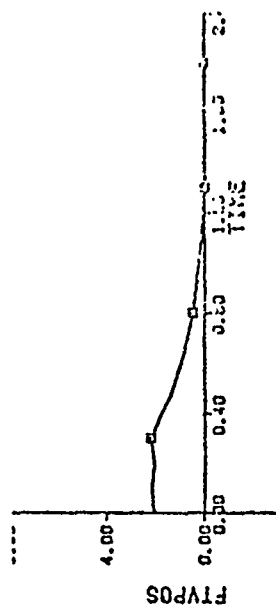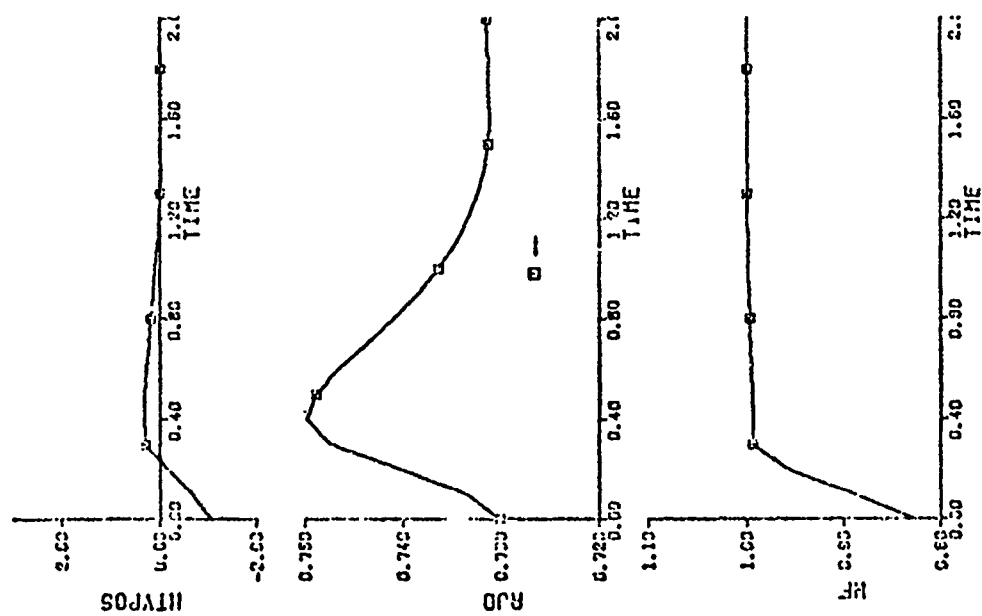
68

Figure 13.   (continue)

69

Figure 13. (concluded)

rotor speeds remain essentially constant, fuel flow is increased to raise turbine temperature, the turbine nozzles (HTVPOS and FTVPOS) are positioned to maintain compressor and fan operating points, and core exhause nozzle (AJC) is closed down to build up PT7 and increase thrust. Intermediate thrust is reached in about one second.

Figures 11, 12, and 13 show clearly that the multivariable controller described in this report is capable of controlling the VCE nonlinear model during large or small transients and steady state, as well or better than the less complicated original F100 engine. The multivariable controller was designed for a single operating condition and adapted to a nonlinear model from which the linear models were derived. In an actual application the controller would have to operate at many different flight conditions on an engine that might behave differently than the nonlinear model and have misrigged actuators or miscalibrated sensors. To study how these factors are handled by the multivariable controller, transient responses (PLA = 20 to PLA = 83) were run for various cases of implanted faults. The steady state results are tabulated in Table 10 and discussed below. The affect on transient response for all the cases was insignificant. For comparison two of the cases were run on the original F100 nonlinear model.

All engine controls require some sensor inputs so the controller can properly position the control actuators. Of importance to the control designer is the impact of sensor errors on critical output parameter response. The multivariable controller presented in this report uses four sensed values (N1, N2, PT7, PT6c). These four sensed values along with the seven calculated control actuator values are fed back to calculate the rate of change of the control actuators. To simulate the

71

TABLE 10

OUTPUT PARAMETER CHANGES FOR DIFFERENT IMPLANTED FAULTS-

VCE AND ORIGINAL F100 NONLINEAR MODEL (PLA=20 TO PLA=83)

Change from base case (steady state)	N2*.97	PT7*.97	WF-300. pph	AJD-.1 sq.ft.	HTVPOS-.5°	RCVV+4°	-2% turbine efficiency	-1.# bleed extraction	RCVV+4° original F100	-2% turbine efficiency orig.F100
% FN	-.3	-.3	1.5	-1.9	-.2	-.3	-.6	-.9	-10.6	-4.3
% TT4M	.2	.2	1.1	1.3	0.	.5	.2	.4	-1.7	-.6
% WFAN	.3	-.3	.3	.2	0.	-.5	-.1	-.2	.3	-1.2
%SMAF	1.8	0.	.7	5.5	-.2	-2.	-.7	-.2	7.5	.6
% SMHC	.4	0.	.3	.8	.8	.3	-1.5	.5	.6	-1.5

effect of a sensor error the sense value of N2 and PT7, going into the controller, were multiplied by 0.97 one at a time. The multivariable controller now has a 3% error in one out of eleven values that determine rates of change of the seven control actuators. If the actuators are adjusted to zero out the error in this one sensor then errors would appear in the other ten feedback terms. If the gain term for the sensor with the error is small compared to the sum of the other 10 gain terms the effect on controller output will be minimal. For the two sensors selected this was the case. Table 10 shows minimal changes in the output parameters for N2 and PT7 sensors errors of 3%.

Another consideration for the control designer is actuator positioning errors. These errors tend to have a greater impact on the output parameters because the feedback gain matrix weights the actuator terms more than the state sensor terms. In fact, one of the basic assumptions made in the development of the multivariable control was that the seven control actuator positions did not have to be measured. The calculated position is fed back and the actual positioning is assumed to be correct. To determine the affect on the output parameters for actuator positioning errors, the nonlinear model was run with various positioning errors introduced. The actuator errors simulated were fuel flow (WF), fan duct nozzle area (AJD), high turbine nozzle area (HTVPOS), and compressor vane position (RCVV). The errors were simulated by subtracting the amount shown in Table 10 from the calculated position and feeding this back to the controller. WF and AJD errors had the largest effect on the output parameters. A 300 pound-per-hour error in WF is equal to about 3% at intermediate power setting and the resulting 1.5% change in thrust is not unreasonably large. The original F100 control schedules a

73

turbine temperature and adjusts WF to hold this temperature. Therefore a fuel flow error would have no affect. But the temperature measurement accuracy is ±0.5% which can cause a variation in FN of about 1.5%. The RCVV error was handled with little difficulty by the multivariable controller. The full transient response for this case is presented in Figure 14 with the base transient for PLA = 20 to 83. For comparison Figure 16 shows the effect of this same error on the transient and steady state response of the original F100 model. As shown in Table 10 this error has a very large effect on the output parameters.

A basic assumption of the multivariable control is that the linear model used to derive the feedback gains accurately represents the actual system. Some of the mechanisms that can change the model are component efficiency deteriorations, changes in airflow pumping characteristics, pressure loss changes, or external extractions of compressor bleed or horsepower. Current turbine engine controls require some sort of retrimming of one or more control schedules when component changes occur. External extractions usually are not accounted for and result in changes to the output parameters. Two of these mechanisms were simulated on the VCE model and one of them on the original F100 model with the results presented in Table 10. In one case high turbine efficiency was reduced by 2%. The VCE multivariable control handled this change to the model with only minor changes to the output parameters whereas the original F100 control allowed FN to change by 4.3%. The transient responses for a high turbine efficiency change for both models is shown in Figures 15 and 17. The other mechanism studied was compressor bleed air extraction of 1 lb./sec. Again the multivariable control was able to handle this with considerably less effect on FN than the original

74

F100 control (0.9% change vs. 2.2%).

As a final item Figure 18 shows the response of the output parameters for a reduced feedback gain matrix. This reduction was discussed in Subsection III-5 and was carried out to show to what extent the optimal control law gains could be reduced and still maintain the same transient response. The original feedback gain matrix had 77 terms, while the reduced matrix had only 33 with no change in the output parameters. The method used to reduce the number of terms was to calculate the percentage contribution of each term on the seven different actuators and retain the largest terms that added up to a preselected percentage. This method required little trial and error but further reductions could probably be obtained using the method detailed in Reference 13.
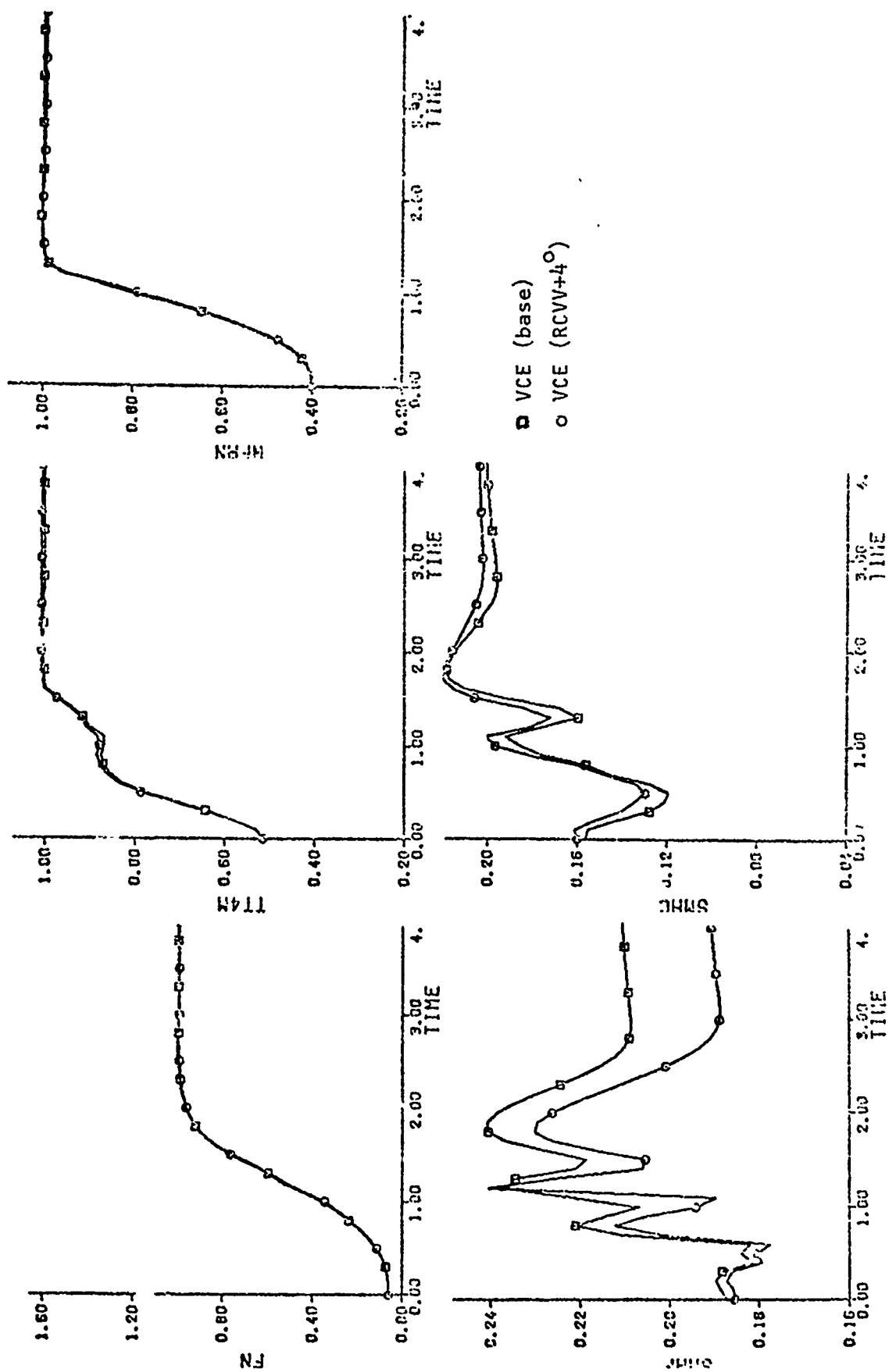
Figure 14. RCVV Actuator Error Effect on VCE Nonlinear Model (PLA=20 to PLA=83)
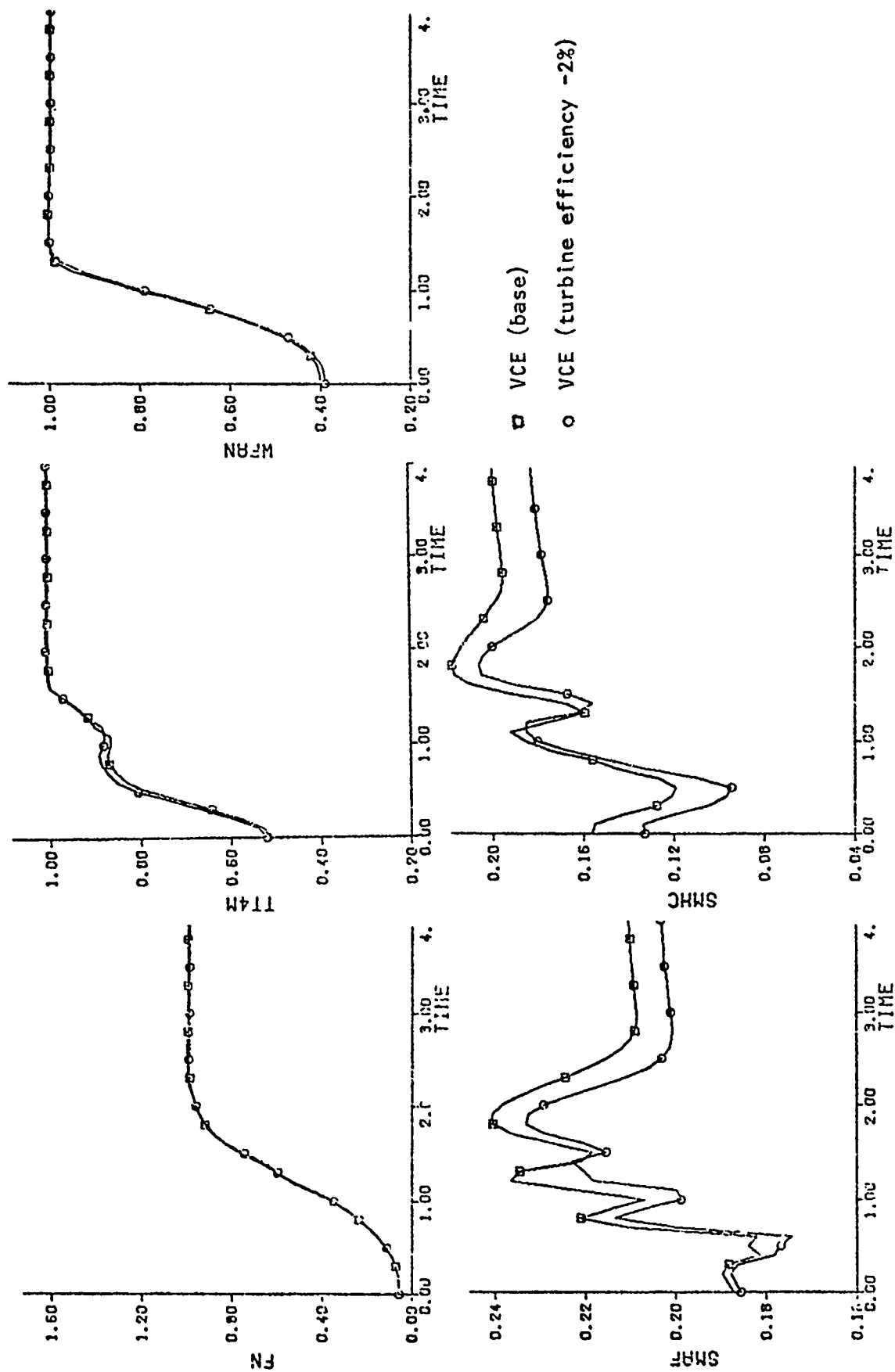
76

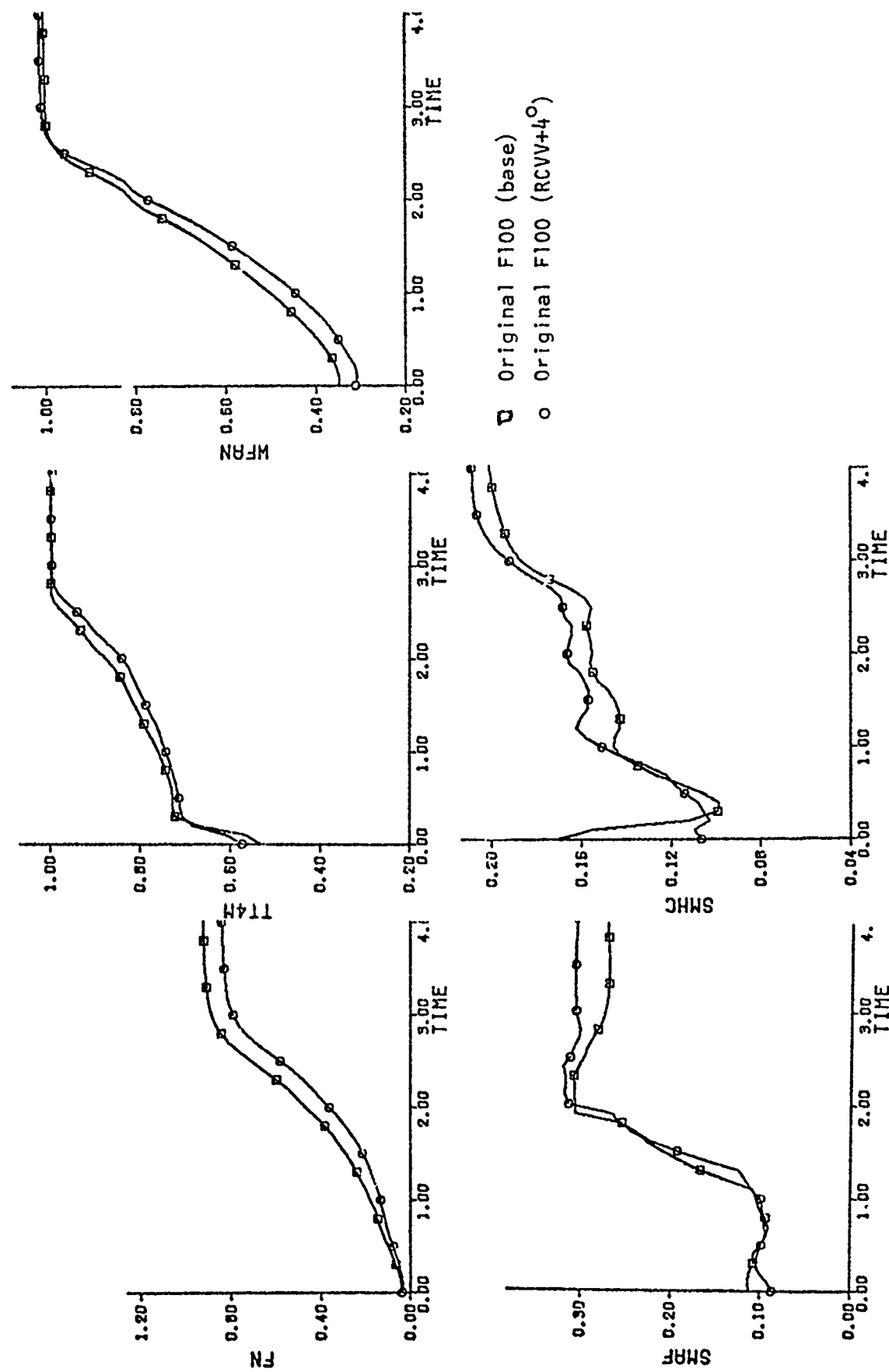Figure 15. Turbine Deterioration Effect on VCE Nonlinear Model (PLA=20 to PLA=83)

77

Figure 16. RCVV Actuator Error Effect on Original F100 Nonlinear Model (PLA=20 to PLA=83)

Original F100 (base)
Original F100 (RCVV+4°)
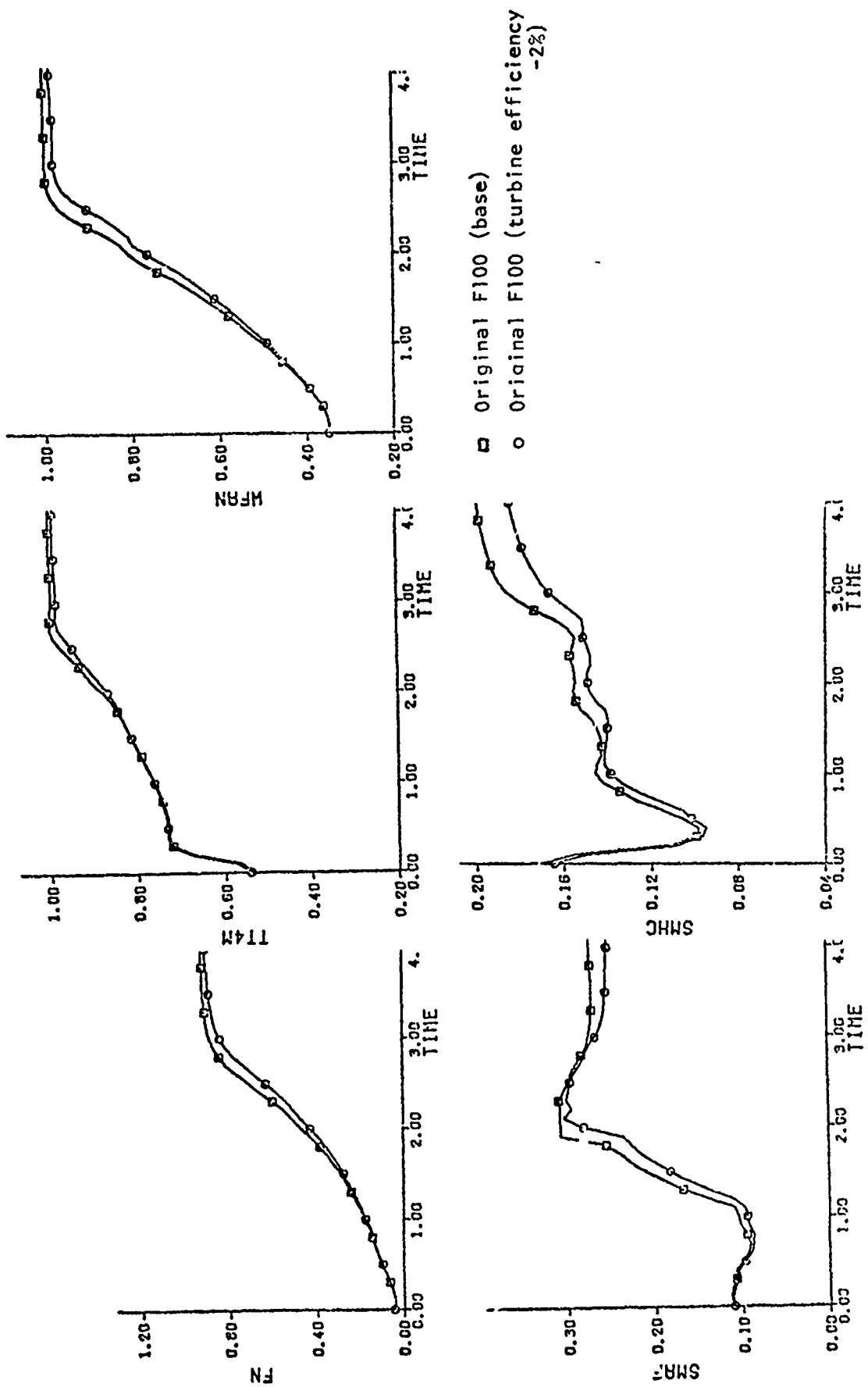
Figure 17. Turbine Deterioration Effect on the Original F100 Nonlinear Model (PLA=20 to PLA=83)

Original F100 (base)
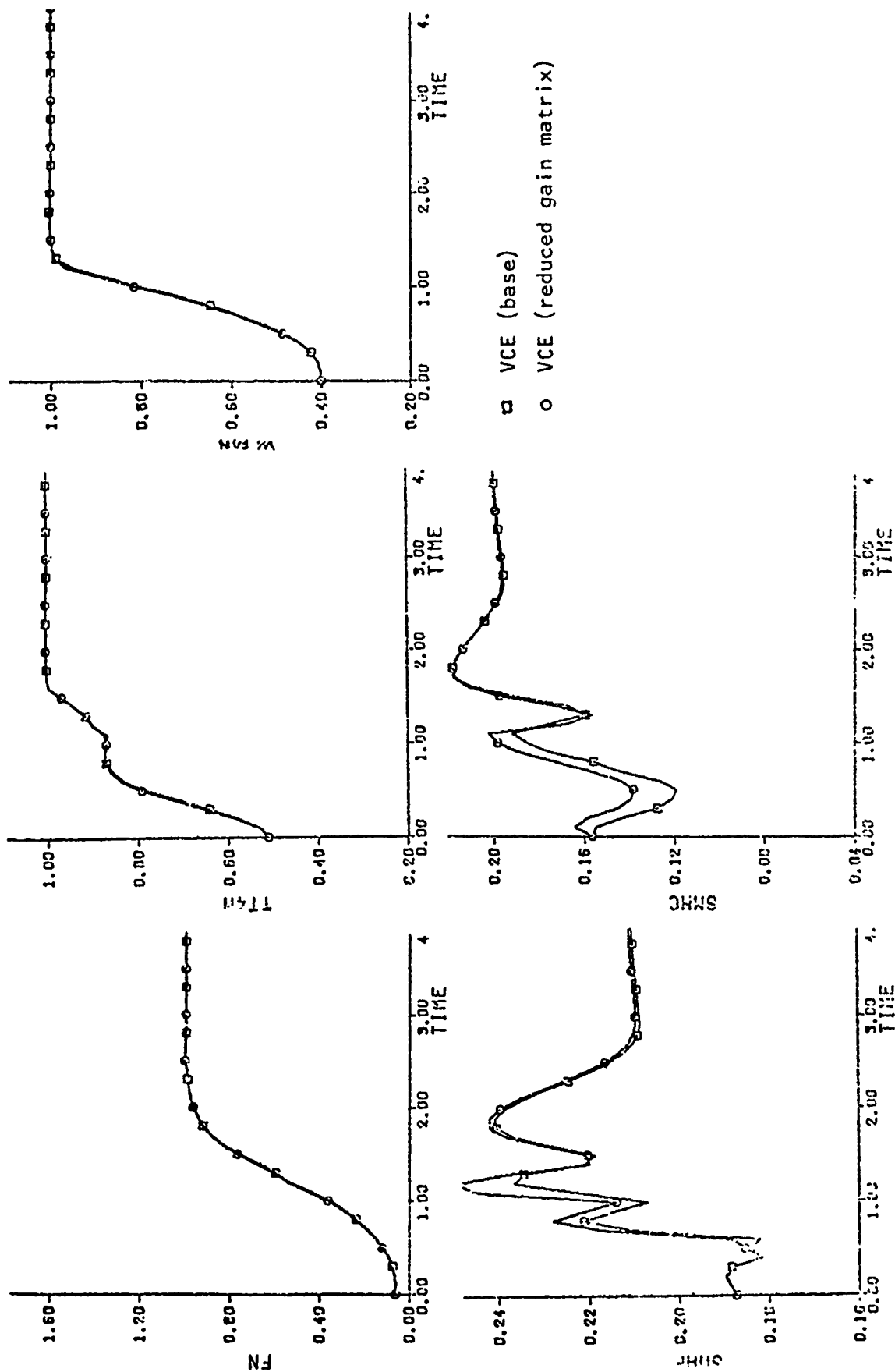Original F100 (turbine efficiency -2%)

79

Figure 18. Reduced Feedback Gain Matrix Effect on the VCE Nonlinear Model (PLA=20 to PLA=83)

80

SECTION V

CONCLUSIONS AND RECOMMENDATIONS

This study has demonstrated the usefulness of linear quadratic regulator theory as a design tool in developing a controller for a multi-input multi-output system. Without such a tool it would be very difficult and time consuming to calculate all of the feedback gain terms, accounting for all the cross coupling effects neces. ry to take full advantage of the additional control input variables provided by a variable cycle engine (VCE) configuration. This is not to say that a controller developed using classical control techniques could not provide the same transient and steady state performance, but that the time, effort and intuition required can be significantly reduced using the approach described in this report.

The interactive graphics program developed in this report solves the Ricatti equation for a user chosen performance index, calculates the feedback gain matrix and displays the transient response of the output, state and input variables on-line. This greatly reduces the time and guessing required to develop values for multivariable gain terms by providing a systematic method for calculating all of the cross-coupling effects. In addition, the control designer has a good idea of what the actual transient response of the engine will be.

The controller developed in this report is capable of controlling the VCE nonlinear model for both transient and steady state at the sea level operating condition, for both large and small step changes in the requested thrust level and within the same constraints imposed on the original F100 model. The transient response times were considerably better than the original F100 model owing to both the multivariable control concept and the inherent capabilities of the VCE concept. The

81

transient responses were similar to published results for similar engine cycles. The steady state variations in the output due to "real" world effects were also handled considerably better by the multivariable controller than by the original F100 model. This was due to the different set of control variables used by the multivariable controller and the inherent capability of the multivariable controller to compensate for variations in the system.

The controller developed in this study was suitable only for the sea level static condition. Further work should be directed toward the calculation of gain matrices that would cover the entire flight envelope. This would require improved gain transitioning algorithms and steady state control schedules. Also, further studies into the many "real world" mechanisms that customarily affect turbine engine o eration should be performed. A method will also have to be developed which allows optimization of the feedback gains on the nonlinear model and the actual engine. That is, if the feedback gain matrix calculated from linear models does not control the actual engine properly, a method must be available to determine which terms of the gain matrix have to be changed and by how much. A future study effort should also determine if a turbine temperature sensor is necessary to safely control a turbine engine. Sensor and actuator dynamics should also be simulated to better represent the actual engine.

REFERENCES

1. Beattie, E. C., Control Mode Studies for Advanced Variable-Geometry Turbine Engines, AFAPL-TR-75-7, Nov 1974.

2. Bowles, R. J., Sub-Optimal Control of a Gas Turbine Engine, Thesis for Air Force Institute of Technology, December 1973.

3. Merril, W. C., An Application of Modern Control Theory to Jet Propulsion Systems, P.H.D. Dissertation for University of Toledo, 1975. (also NASA TM X-71726)

4. Michael, G. J., Farrar, F. A., Development of Optimal Control Modes for Advanced Technology Propulsion Systems, United Aircraft Research Laboratories Report, M911620-1, August 1973.

5. Michael, G. J., Farrar, F. A., Development of Optimal Control Modes for Advanced Technology Propulsion Systems, United Aircraft Research Laboratories Report, N911620-2, March 1974.

6. Weinberg, M. S., A Multivariable Control for a Turbofan Engine Operating at SLS, ASME 76-GT-71 or ASD-TR-75-28.

7. Beattie, E. C., Application of Multivariable Optimal Control Techniques to a Variable Area Turbine Engine, Purdue University, Joint Automatic Control Conference Proceedings, July 1976.

8. F100-PW-100 (3) Transient Engine Simulation Deck User's Manual for Deck CCD 1078, Pratt and Whitney Aircraft, Government Products Division, FR-6014, October 1973.

9. May, R. J., et. al., Influence of Variable Turbine Geometry on Engine Installation Losses and Cycle Selection, AFAPL-TR-73-18, 1973.

10. Weinberg, M. S., Adams, G. R., Low Order Linearized Models of Turbine Engines, ASD-TR-75-24, 1975.

11. Kirk, D. E., Optimal Control Theory, Prentice-Hall Inc., Englewood Cliffs, New Jersey, 1970.

12. Weinberg, M. S., Direct Reduction of High Order Linear Systems by State Variable Techniques, ENJE-TM-75-6, 1975.

13. Michael, G. J., Sagliero, G. S., Key Control Assessment for Linear Multivariable Systems, Report R76-942042, Air Force Office of Scientific Research, January 1976.

APPENDIX A

DERIVATION OF NOZZLE POSITIONING
FOR VARIATIONS IN TURBINE INLET TEMPERATURE

Two basic equations will be used to derive relationship: for the three areas (A4, A45, and A8, equivalent to HTVPOS, FTVPOS, and AJC) as T4 (1T4M) is varied to modulate thrust while a constant match of the fan and compressor is maintained. Airflow (WG4), pressure (PT4) and the work (Δh) across the turbines will be nearly constant because of the constant match of the fan and compressor.
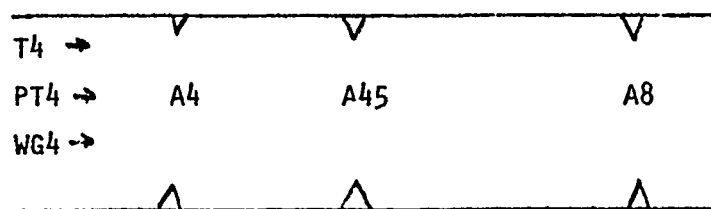
Starting at Station 4 (high pressure turbine) and assuming for simplicity the turbine efficiencies (η) remain constant, the first two equations are:

$$\Gamma_4 = WG4 \ (T4)^{\frac{1}{2}} \ / \ (PT4 \ A4) = K1 \tag{A-1}$$

$$\Delta h = \eta \ \Delta h_{id} = \eta \ C_p \ T4 \ (1 - (PT45 \ / \ PT4)^{(\gamma-1)/\gamma}) = K2 \tag{A-2}$$

$$= \eta \ C_p \ T4 \ (1 - T45 \ / \ T4) = K2$$

The relationship for A4 is obtained directly from Equation A-1;

$$A4 = K3 \ (T4)^{\frac{1}{2}} \qquad \text{where} \quad K3 = WG4 \ /(PT4 \ K1) \tag{A-3}$$

The relationships between T4 and Pt45 and T45 are obtained by rearranging Equation A-2;

$$PT45 \ / \ PT4 = (1 - K2 \ / \ (\eta \ C_p \ T4))^{\gamma/(\gamma-1)}$$

or

$$PT45 = PT4 \ (1 - K4 \ /T4)^{\gamma/(\gamma-1)} \qquad \text{where} \quad K4 = K2 \ /(\eta C_p) \tag{A-.}$$

84

Rearranging and substituting for PT45 / PT4;

$$T45 = T4 - K2 / (\eta\, C_p) = T4 - K4 \qquad\qquad\qquad \text{(A-5)}$$

Continuing to station 45 (fan drive turbine) and using the same basic equation;

$$\Gamma45 = WG45\,(T45)^{\frac{1}{2}} / (PT45\; A45) = K5 \qquad\qquad \text{(A-6)}$$

$$\Delta h = \eta\, \Delta h_{id} = \eta\, C_p\, T45\, (1- (PT5 / PT45)^{(\gamma-1)/\gamma}) = K6 \qquad \text{(A-7)}$$
$$= \eta\, C_p\, T45\, (1 - T5 / T45) = K6$$

Rearranging Equation A-6 and substituting for PT45 and T45 from Equations A-4 and A-5, A45 is obtained;

$$A45 = WG45\,(T45)^{\frac{1}{2}} / (PT45\; K5) = (K7\,(T4-K4)^{\frac{1}{2}}\, T4^{\gamma/(\gamma-1)}) / (PT4\,(T4-K4)^{\gamma/(\gamma-1)})$$

$$\text{where;}\quad K7 = WG45 / K5 \qquad\qquad \text{(A-8)}$$

PT5 is obtained from Equation A-7 by substituting in Equations A-4 and A-5

$$PT5 / PT45 = ((1 - K6 / (\eta\, C_p\, T45))^{\gamma/(\gamma-1)}$$

or

$$PT5 = (1 - K4 / T4)^{\gamma/(\gamma-1)}((1- K8) / (T4 - K4))^{\gamma/(\gamma-1)} \qquad \text{(A-9)}$$

$$\text{where}\quad K8 = K6 / (\eta\, C_p)$$

$$T5 = T45 - K6 / (\eta\, C_p) = T4 - K9 \quad \text{where } K9 = K4 + K8 \qquad \text{(A-10)}$$

The relationship for the core nozzle area A8 is derived assuming a choked nozzle and a constant pressure drop across the tailpipe.

$$\Gamma8 = (WG8\; T8^{\frac{1}{2}}) / (PT8\; A8) = K10 \qquad\quad WG8 \text{ is constant} \qquad \text{(A-11)}$$
$$PT8 = PT5\,(1 - K11)$$
$$T8 = T5$$

rearranging;

$$A8 = K12\; T5^{\frac{1}{2}} / PT5 \qquad\qquad\quad \text{where}\quad K12 = WG8 / (K10\,(1-K11))$$

$$A8 = (K12\,(T4 - K9)^{\frac{1}{2}}) / (PT4\,(1-K4/T4)^{\gamma/(\gamma-1)}\,(1-K8/(T4-K4))^{\gamma/(\gamma-1)})$$

$$\text{(A-12)}$$

Assuming some typical values, for the constants, the three areas can be calculated for various values of T4.

85

$WG4 = 117.2$ $WG45 = 140.9$

$PT4 = 354.7$ $K5 = 67.1$

$K1 = 18.2$ $\dot{n}45 = .903$

$n4 = .888$ $C_p 45 = .29$

$C_F 4 = .30$ $K6 = 97.6$

$K2 = 227.$ $WG8 = 141.7$

$\gamma = 1.345$ $K10 = 132.7$

$\qquad\qquad\qquad$ $K11 = .038$

Using these values, Equations A-3, A-8 and A-12 were evaluated for various values of T4 and plotted in Figure Al with the actual areas from the nonlinear simulation. The areas are relative to their intermedia e level values.
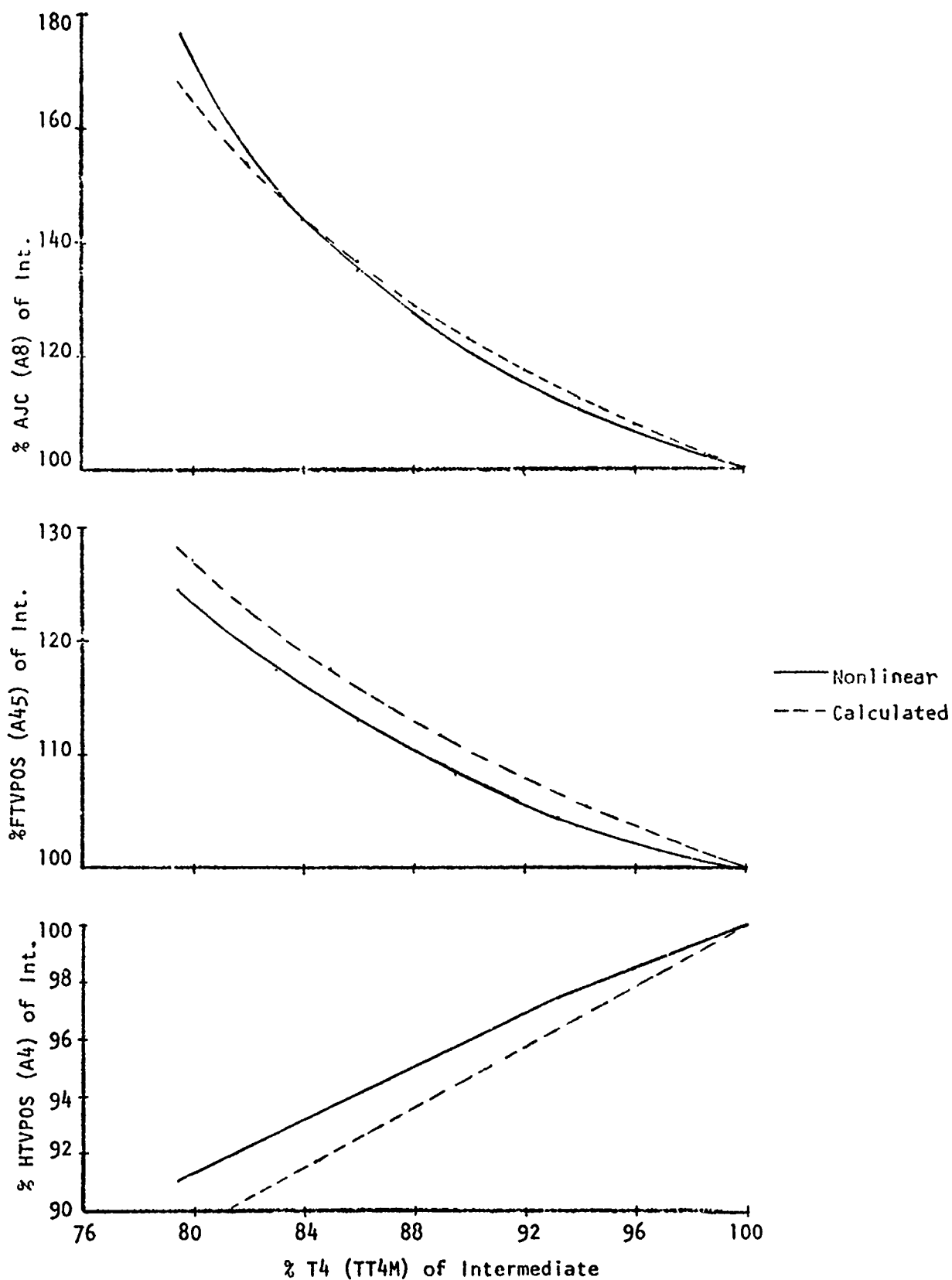
Figure A-I. Variation in Areas with Turbine Temperature

87